Winter 12-2018

Numerical Simulation and Optimization of Blalock-Taussig Shunt

Thomas Hess
Washington University in St. Louis

Ramesh K. Agarwal
Washington University in St. Louis

WASHINGTON UNIVERSITY IN ST. LOUIS
School of Engineering and Applied Science
Department of Mechanical Engineering and Materials Science

Thesis Examination Committee:

Dr. Ramesh K. Agarwal, Chair

Dr. David Peters

Dr. Spencer Lake

Numerical Simulation and Optimization of Blalock-Taussig Shunt

by

Thomas Hess

A thesis presented to the School of Engineering and Applied Science
of Washington University in St. Louis in partial fulfillment of the
requirements for the degree of
Master of Science

December 2018

Saint Louis, Missouri

Content

List of Figures

List of Tables

Nomenclature

BT Shunt	Blalock-Taussig Shunt
CAD	Computer-Aided Design
CFD	Computational Fluid Dynamics
CPU	Central Processing Unit
DH	David Hoganson
FDM	Finite Difference Method
FEM	Finite Element Method
FVM	Finite Volume Method
GGNB	Green-Gauss Node-Based
HHA	Hess-Hoganson-Agarwal
IA	Innominate Artery
LPA	Left Pulmonary Artery
PDE	Partial Differential Equation
RPA	Right Pulmonary Artery
WSS	Wall Shear Stress

Acknowledgments

I would especially like to thank Dr. Ramesh Agarwal for his continuous support and guidance from the start of this project. He has provided his extensive wisdom within and outside of my studies and inspired me with his passion for his occupation and for his students.

I would like to thank Dr. David Hoganson of Boston's Children's Hospital for his perpetual support and time spent working on the project and expertise in the medical side of BT shunts.

I would also like to thank my father, Dr. Jeffery Hess, for his time spent explaining and teaching medical jargon on a regular basis. As well as my mother, Dr. Lori Hess, for support only a mother can bring and proof reading of this paper.

Thank you to my colleagues in the CFD labs, especially Jeff Krampf, who are always willing to lend a helping hand.

Finally, I would like to thank Washington University in St. Louis and the NASA-Missouri Space Grant Consortium for this opportunity to research.

Thomas Hess

Washington University in St. Louis
December 2018

Dedicated to my family.

ABSTRACT

Numerical Simulation and Optimization of Blalock-Taussig Shunt

by

Thomas Hess

Master of Science in Mechanical Engineering

Washington University in St. Louis, 2018

Research Advisor: Professor Ramesh K. Agarwal

The goal of this study is to create an optimized Blalock-Taussig shunt used to temporarily repair pulmonary vascular blockages allowing a child time to grow so a more permanent surgical repair of the heart and vasculature can be performed. Blalock-Taussig or BT shunts are a surgical procedure performed on infants suffering from cyanosis or "Blue Baby Syndrome." A BT shunt is an artificial vessel placed between the right ventricle and the pulmonary artery to increase blood flow in the lung and blood oxygen saturation levels. In a study of 96 patients with currently in use modified BT shunts, 32 patients (21%) had greater than 50% stenosis caused by myofibroblastic proliferation at the shunt lumen due to shunt geometry [1]. A 2007 study by the cardiac surgery division of Johns Hopkins Medical Institutions found an operative mortality rate of 14% (227 of 1,574) with patients undergoing BT surgery [2].

In this thesis, the flow of blood through several different BT shunt configurations from actual patient data was analyzed using the commercial CFD software ANSYS Fluent. Results from each shunt's analysis were then compared to determine the shunt parameters with optimal flow dynamics for use in infants suffering from pulmonary vascular blockage. It was found that the entrance boundary of current BT shunts caused blood flow hindrances due to high wall shear values and flow separation. A newly designed shunt was proven to partially fix this problem; however, a superior model could be optimized by using characteristics from currently used shunts and CFD results. Many iterations and designs of BT shunts were made using Solidworks, a solid modeling computer-aided design program, and were tested using Fluent to create a shunt optimized by smoothening the transition between areas of high and low wall shear stress, lowering the overall maximum wall shear stress, reducing flow separation, and equalizing the flow to the left and right lung. All these factors contribute to the chance of thrombosis and morbidity within patients. The resultant model shunt showed drastic improvement in lowering the average wall shear stress by more than 85% at the initial boundary with over 20% drop in overall average wall shear. It also achieved a decline of the maximum wall shear stress by over 25% while negating the possibility of any flow separation and improving the equality in flow to the left and right lung by more than 60%.

Chapter 1 Introduction

1.1 Overview

1.1.1 Blalock-Taussig (BT) Shunt

Blalock-Taussig or BT shunts are a surgical procedure performed on infants suffering from cyanosis or "Blue Baby Syndrome." Cyanosis refers the purple or blue color of the skin resulting from low blood oxygen saturation. Cyanosis in newborns can occur when a child has a congenital heart defect or malformation of blood vessels in heart and lungs such as tricuspid atresia, pulmonary artery constrictions, or atrioventricular defects. Time is needed for these children to outgrow the issues or be eligible for a perennial fix. Therefore, a new vessel is required for a sufficient amount of blood to bypass the defects and reach the lungs for oxygenation.

Originally the Blalock-Taussig (BT) surgery was performed by Dr. Alfred Blalock and Dr. Helen Taussig in 1944 where they conjoined the subclavian artery to the pulmonary artery to direct blood flow back into the patient's lungs. At the time, children with congenial heart defects were at high risk of morbidity or severe developmental issues. Dr. Taussig described one of the early successful operations "*as an utterly miserable, small six-year old boy who was no longer able to walk…the boys a lovely color now*!" and reported the patient turned into a happy, active child [3].

Today, the original procedure is modified to place a BT shunt, an artificial vessel, between the right ventricle and the pulmonary artery instead of sewing the vessels directly together. This increases lung blood flow and blood oxygen saturation levels while allowing follow-up permanent surgeries to be performed easily after growth of the child. A depiction of a standard BT shunt can be seen below in Figure 1.1.

A BT shunt acts a temporary ductus arteriosus, which is a natural shunt in the fetal circulation to bypass the pulmonary vascular system while the lungs are filled with amniotic fluid. After birth, the lungs fill with air and hormones are released causing the ductus arteriosus to constrict, scar, and close forcing blood into the pulmonary vessels to be oxygenated. For children with a blockage of the pulmonary vascular system, such as with pulmonary stenosis, pulmonary atresia, or tricuspid atresia, the ductus arteriosus must remain intact to allow blood to move from the systemic to pulmonary vascular system to be oxygenated. If the ductus arteriosus becomes constricted or closes prematurely, the resulting inability to oxygenate blood will cause cyanosis and eventual death of the infant.

The use of a BT shunt is a temporary palliative procedure taking the place of the ductus arteriosus. The shunt does not completely repair pulmonary vascular blockages but allows the child time to grow so a more permanent surgical repair of the heart and vasculature can be performed. A typical shunt is cylinder made from a synthetic hydrophobic material called Gore-Tex. The cylinder expands from blood pressure similar to a real blood vessel. Typically, BT shunts vary in diameter from 3 to 4 cm depending on size and age of the infant.

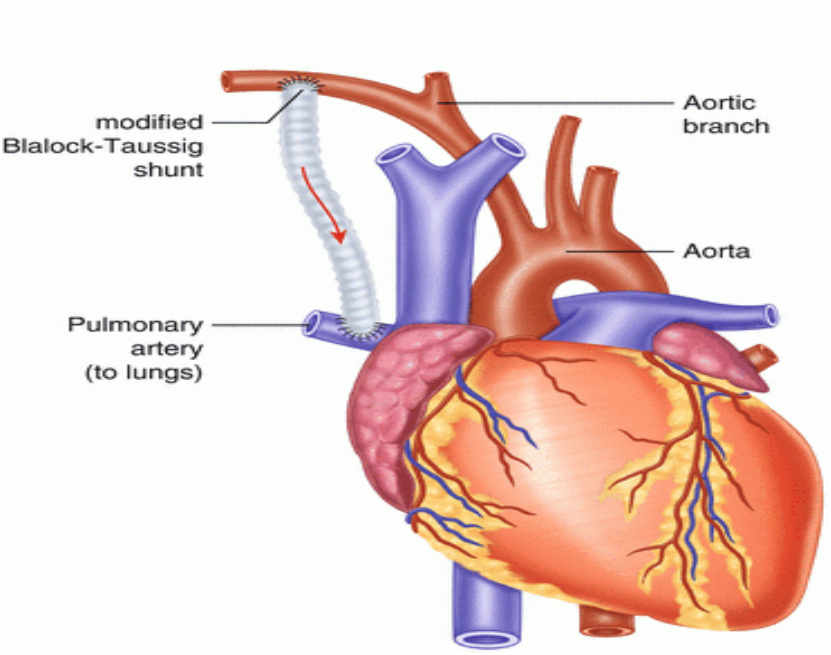

Figure 3.1 Overview of the positioning of a BT shunt [4]

Wall shear stress (WSS) is a main component of determining how well a shunt works in the human body due to its effects on the biological properties of blood. The amount of WSS is determined by many factors such as flow velocity, flow separation, and geometric shape. For instance, areas with high fluctuations in velocity will result in large amounts of shear stress on the walls while areas with flow separation will create a zone of flow stasis or "dead zone" where flow velocity is low or nonexistent. In this dead zone the WSS gradients are very low resulting in negligible WSS. These zones are common at the throat of a stenosis, gaps between mechanical valve edges, or areas with swirling flow. These areas are dangerous due to the possibly of entrapment and aggregation of platelets in the blood.

WSS values and dead zones are important in analyzing blood flow due to their effect on platelets in the blood. When exposed to non-physiological shear rates, such being too low in recirculation zones or too high in the shunt lumen, platelets have a high probability of activating. This activation also largely depends on how long and how often the platelets are exposed to abnormal WSS values.

When a platelet activates it becomes sticky and releases signals for other surrounding platelets to activate. These activated platelets stick to each other as well as other cellular components in the blood forming clots. Clots with a diameter larger than the shunt will become stuck in the shunt forming a thrombosis and stop blood flow. Clots with a diameter smaller than the shunt will travel out into the vascular system and could encounter a small blood vessel they could block forming a thrombosis or causing tissue damage.

Once activated, platelets have a high tendency to aggregate but require a conducive environment such as an area of low WSS where the velocity magnitude is low. If platelets are entrapped in a circulation zone there is a much higher probability more platelets will aggregate and a clot or stenosis to form. Therefore, a quick transition from high WSS to low WSS are the even more dangerous than areas of high WSS since high WSS areas have the ability to "wash" the platelets off.

Thus, an ideal new shunt design will smoothen the transition between areas of high and low wall shear stress, lower the overall maximum wall shear stress, reduce flow separation, and equalize the flow to the left and right lung. Larger shunts have greater flowrates and lower maximum WSS, however, the size of shunt that can be use is dependent on patient conditions such as vessel area available for surgery.

1.1.2 Motivation

While great improvements have been made involving the surgery by developing material to be used as artificial vessels or tools used in assistance to the surgeon, the fluid dynamic properties and shape of the shunt has been largely overlooked. This thesis serves to fulfill these needs and stretch the bounds of what a BT shunt looks like. The goal of this dissertation is to retain necessary properties such as effective resistance (EF) and biological shape restraints while optimizing the shape for lowering the maximum WSS, smoothing the transition between areas of high and low WSS, minimizing flow separation, and equalizing the blood flow to the left (LPA) and right (RPA) pulmonary arteries. These models are designed using CAD software Solidworks while flow properties are examined using CFD software ANSYS Fluent. Since the number of variables within the shunt models are much higher than previous studies of BT shunts, the numerical and qualitative data are used for trial and error-based optimization.

1.2 Brief Review of Literature

BT shunts remain an important topic for study due to numerous unstudied properties and applications as well as a remarkably high chance of morbidity. In a 2011 study, 1273 patients undergoing neonatal Blalock-Taussig surgery were studied to find post-operation risk factors for mortality and morbidity. An overall 13.1% chance of morbidity was found with 33% of deaths occurring within 24 hours and 75% within the initial month. Of the patients, 62% were amenable for a permanent biventricular repair after BT surgery. It was concluded that the mortality rate of neonatal BT shunt surgery remains significantly high, especially for infants weighing less than 3 kg or with a diagnosis of pulmonary atresia with intact ventricular septum (PA/IVS) [5].

Since no available endothelial or muscle fiber tissues are available during operations, modern BT shunts are created using a synthetic material known as Gore-Tex. While older grafts caused areas of non-physiologic flow resulting in stenosis or thrombosis in shunts, Gore-Tex provides a customizable stretch to non-stretch material that can mimic physical properties of blood vessels to improve fluid flow, kink resistance, and shape integrity [6]. Since 1982 Gore-Tex has proven to reduce morbidity with BT patients [7]. Experimental progress has started to adopt umbilical vein segments in place of Gore-Tex material to provide a closer resemblance to blood vessels as well as a lower chance of foreign body rejection.

1.3 Scope of the Thesis

This thesis aims to create a new optimized shape for blood blow through a BT shape while retaining biological constraints. Throughout this study several assumptions are made: the walls of the shunt are smooth and rigid; blood is a Newtonian fluid with a density of 1050 kg/m^3 and viscosity of 0.00255 kg/ms; and the flow boundary conditions are set by an average of accrued patient data. Each model is created and modified in Solidworks while meshed using ICEM CFD, a mesh generation package found within the ANSYS workbench. Fluid analysis is done using ANSYS Fluent while post processing is done using ANSYS CFD Post, an extension of Fluent. Each case is solved using a k-kl-ω turbulence model and a coupled algorithm for solving momentum and pressure equations. Recorded numerical data is imported into Microsoft Excel to be studied and compared.

Chapter 2 Methodology

2.1 Overview

The objective of this dissertation is to produce a new design of BT shunt that achieves: a lower overall maximum WSS, a smooth transition between high and low WSS, a minimal amount of flow separation, an equivalent effective resistance to modern shunts, and finally an even flow distribution to the left and right lung. In order to accomplish this goal, current BT shunts were studied in the form of four case studies to achieve adequate data on modern day shunts. These case studies consisted of four Solidworks CAD files (KC, KS, JJ and CS) along with four boundary conditions provided by surgery data for each. These cases were also solved in standardized form with boundary conditions equal for the 3.5 mm and 4.0 mm shunts respectively.

Once each of the case studies were thoroughly investigated using CFD, an initial model design was created by Dr. Hoganson to completely change the shape of modern-day shunts. This design was proven to be a promising onset of our design goals and our optimization process began there. In the beginning, several different optimization methods were proposed, however the timeline of this dissertation restricted our use of such algorithms and a simple trial and error-based optimization method was chosen based on the sheer number of variables available for change in our models.

Our method for optimization was therefore setup as follows: run the newly created model through meshing and CFD software, move numerical results into excel, create WSS contour and velocity profile photos, analyze numerical and qualitative data, discuss findings of recent changes to model with Dr. Hoganson, and finally make adjustments to the model based on results and discussion. Early on in the optimization process very drastic changes were made to the model in order to easily see how the change in shape effects the overall fluid flow. A diagram of this process is shown below in Figure 2.1 with the program used during each step shown to the right.

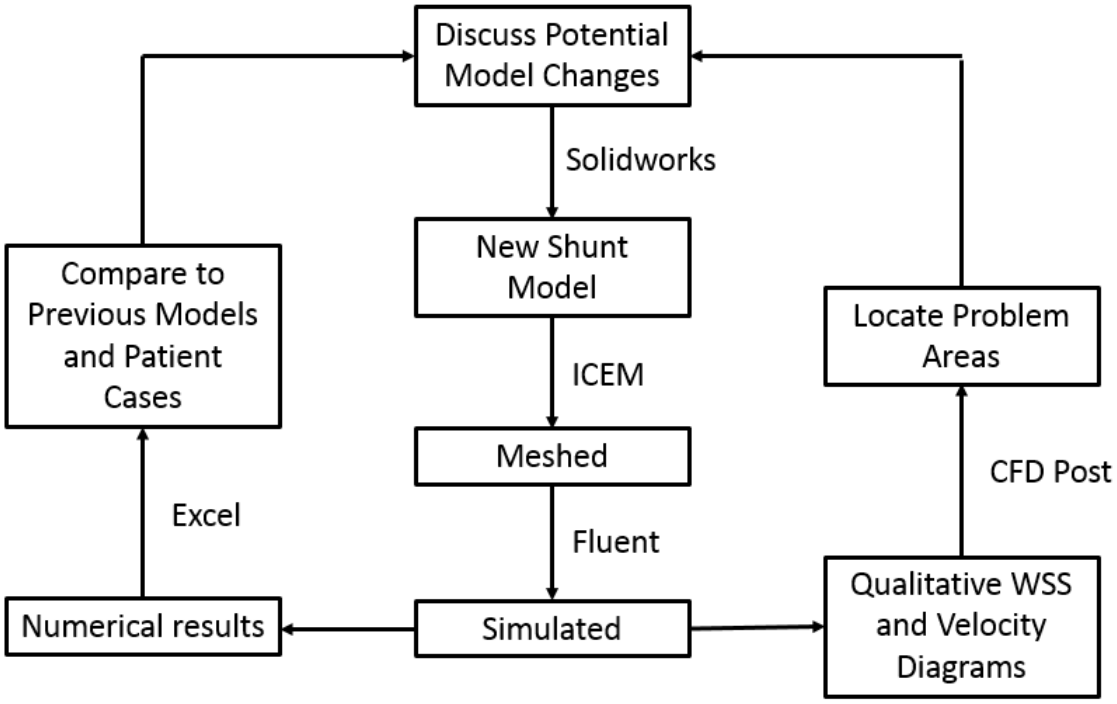

Figure 4.1 Overview of Shunt Optimization Process – Software used during each step shown on the right

2.2 Model Creation

2.2.1 Overview

During each of the two studies, case studies and Hess-Hoganson-Agarwal (HHA) models, CAD models of the shunt are needed to be created and modified for use within ANSYS Fluent. The original four case studies: KS, JJ, KC, and CS are BT shunts currently in use within surgery today and have many CAD models available. The KS and JJ shunts are 3.5mm while KC and KS are 4.0 mm. Each case study CAD model used during this dissertation are shown in Figure 2.2.

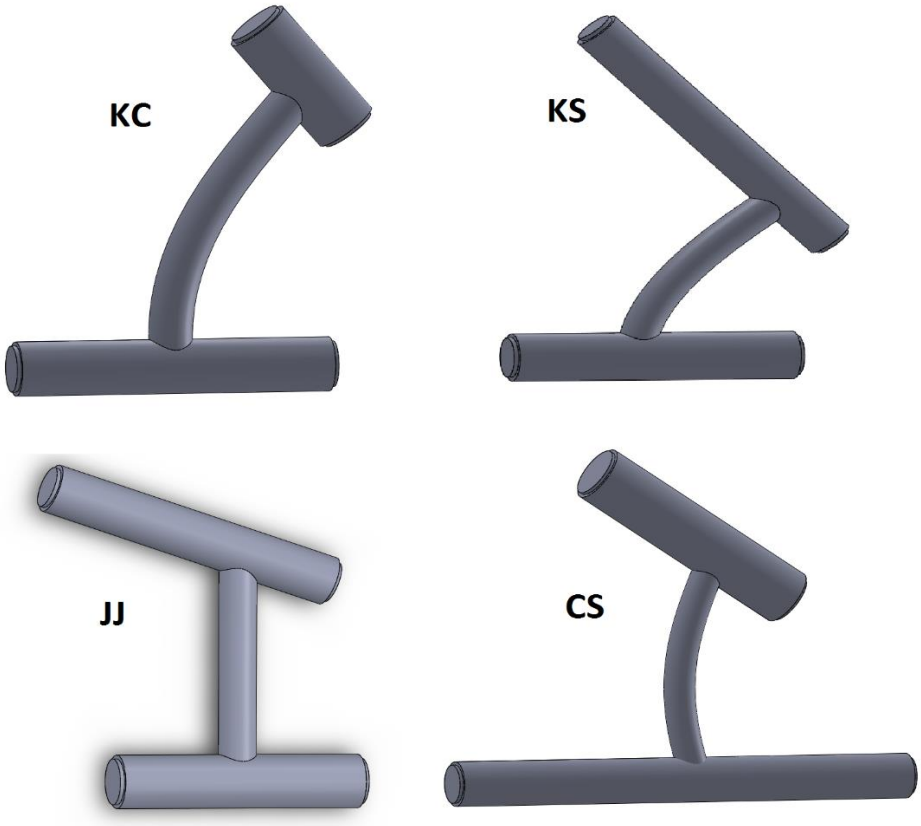

Figure 2.2 Case Studies CAD Models

However, these models are not entirely compatible within fluent as a raw file and must be modified. Rather than having a model of the walls of the shunt, a model of the negative space where blood will be flowing is used within fluent. When Dr. Hoganson created his first model of a new type of shunt (DH shunt), he wanted to better model the biological positioning of the IA and PA and thus used medical data to put them on separate planes by about 3mm as well as angling the IA in a more vertical direction.

All previous CAD models of shunts keep the shunt completely symmetrical about its centerline and on the same plane for simplicity sake. This was done in order to better mimic the differences he saw between the models and when actually performing the surgery as well as provide some unpredictability in the model as each patient will have slightly differing positions of vessels. He also included an offshoot artery on the PA in order to provide reference to the area that the shunt is capable of being sewn in. Dr. Hoganson followed the precedent before him and modeled the walls of the shunt which needed to be modified before study. David Hoganson's initial DH shunt is shown in Figure 2.3.

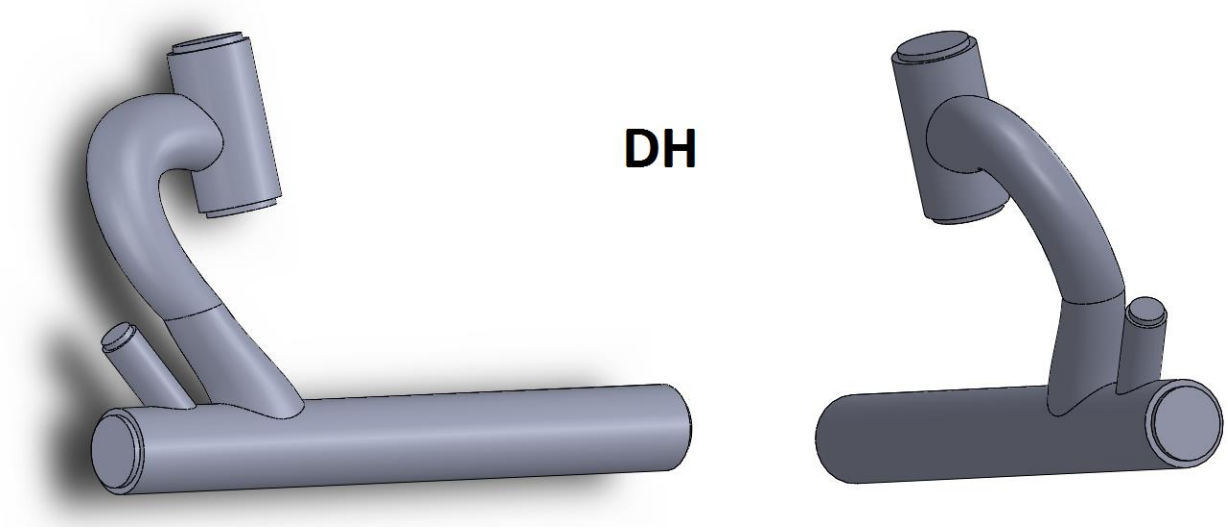

Figure 2.3 David Hoganson's initial DH shunt

When designing the CAD for our new HHA shunts, several changes were made from the standard in order to create a file fully ready to be imported into Fluent as well as much more easily customizable. The changes Dr. Hoganson made to the biological positions of the IA and PA were kept in all HHA models, however the PA offshoot was deemed unnecessary to model. However, the position of this offshoot is still important due to its limiting factor of how far towards the RPA the shunt can be attached. Various mechanical and stylistic problems were fixed from the DH model, but the general shape was preserved. The Solidworks file was fully dimensionalized to allow length measurements to be taken to create a database of changes between shunt models as well as used in various equations later in the excel analysis. In order to create a new iteration of HHA shunt, any one of the 50+ different variables can be easily changed to the desired length, size, or position and would immediately be ready for fluent analysis. An example geometry of an HHA shunt designed in this dissertation is shown in Figure 2.4.

Figure 2.4 Example of an HHA geometry: HHA v1.3.3

2.2.2 Case Study Model Modifications

For each of the five case studies, including the initial DH design, a CAD model along with boundary conditions, acquired from averaging patient data, was provided by Dr. Hoganson. However, the given CAD files were incompatible with Fluent because pipe-flow analysis wants the solid geometry of the volume the fluid is moving through, not the pipe walls themselves. Therefore, each shunt had to be "de-shelled" in order to create the appropriate geometries.

First, all outer faces were deleted on the geometry using the face delete function in Solidworks. This results in a shell of the boundary the fluid flows through but is needed to be a filled solid. A single face on this shell is deleted and re-added using the planar surface function in order to create to separate objects. Then, the knit function can be used between the shell and re-added surface in order to recreate a single object. During this, "create solid" can be selected to fill the innards of the shell into a solid. An example of a starting and de-shelled geometry is shown in Figure 2.5.

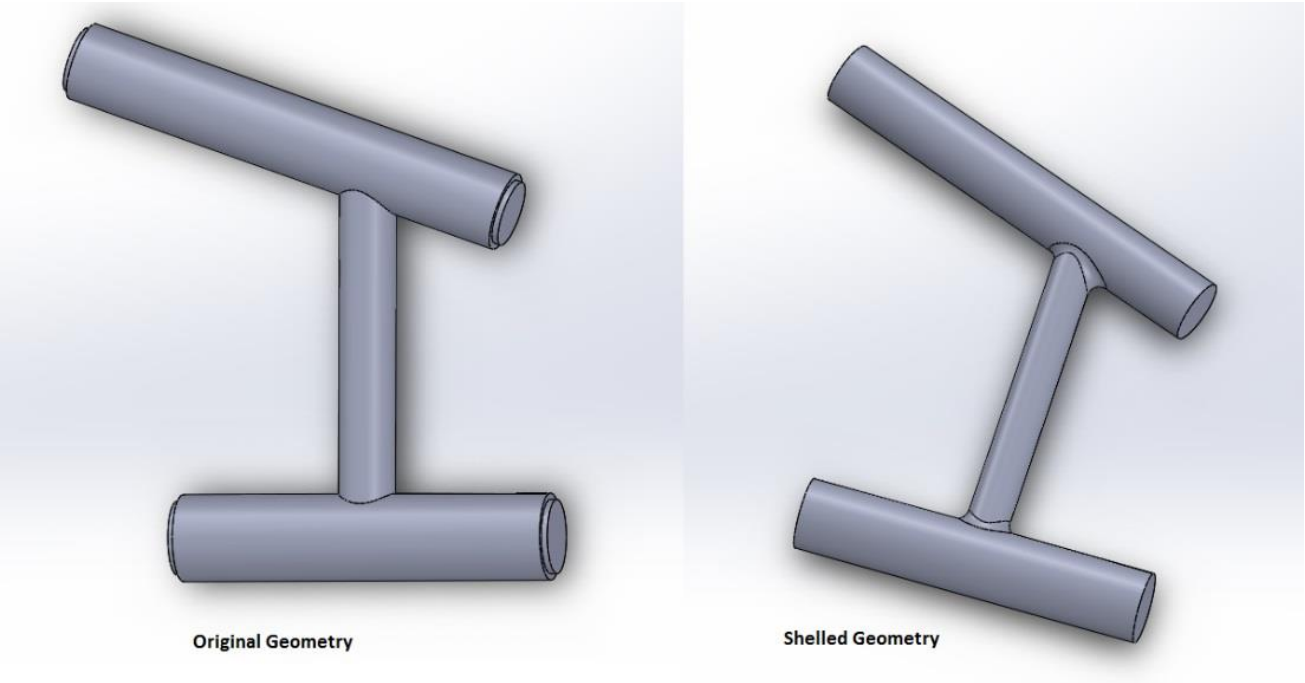

Figure 2.5 Geometry Modifications for JJ Case Study File

2.2.3 Hess-Hoganson-Agarwal (HHA) Model Creation

After reviewing the results from the initial DH design, it was clearly shown that its shape was more optimized for fluid flow than the current day shunts, but further modification is needed. The HHA CAD was created from scratch in order to eliminate the need for de-shelling by modeling the fluid space while also keeping planes / sketches to a minimum and variables deemed important easily changeable. Every plane and sketch was labeled to ease communication over the design and allow variables to be easily found for modification. Many of the biological measurements started in the DH shunt were remade in HHA models, however several large changes were necessary between the HHA and DH designs.

First, the angle at which the shunt connects to the IA and PA were modeled as planes for the shape of the entrances to be sketched onto. This allows both the angle and shape of both connections to be customizable rather than static. Next, in the initial DH design two separate extrusions were used to form the shunt geometry that created an abrupt transition unfit for smooth fluid flow as shown in Figure 2.6.

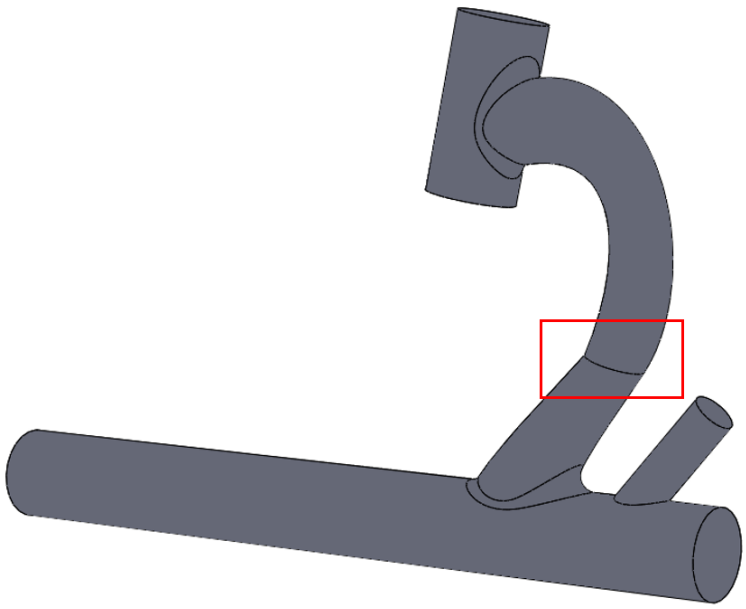

Figure 2.6 Initial DH Design Flaw

This problem was fixed in HHA models by creating a single extrusion by using two guide splines in an boundary-boss extrusion. These splines were created using two points each which allow for nearly infinite shape configurations when combined with editing the customizable IA and PA connections. A photo of how the splines can be edited in Solidworks is shown in Figure 2.7.

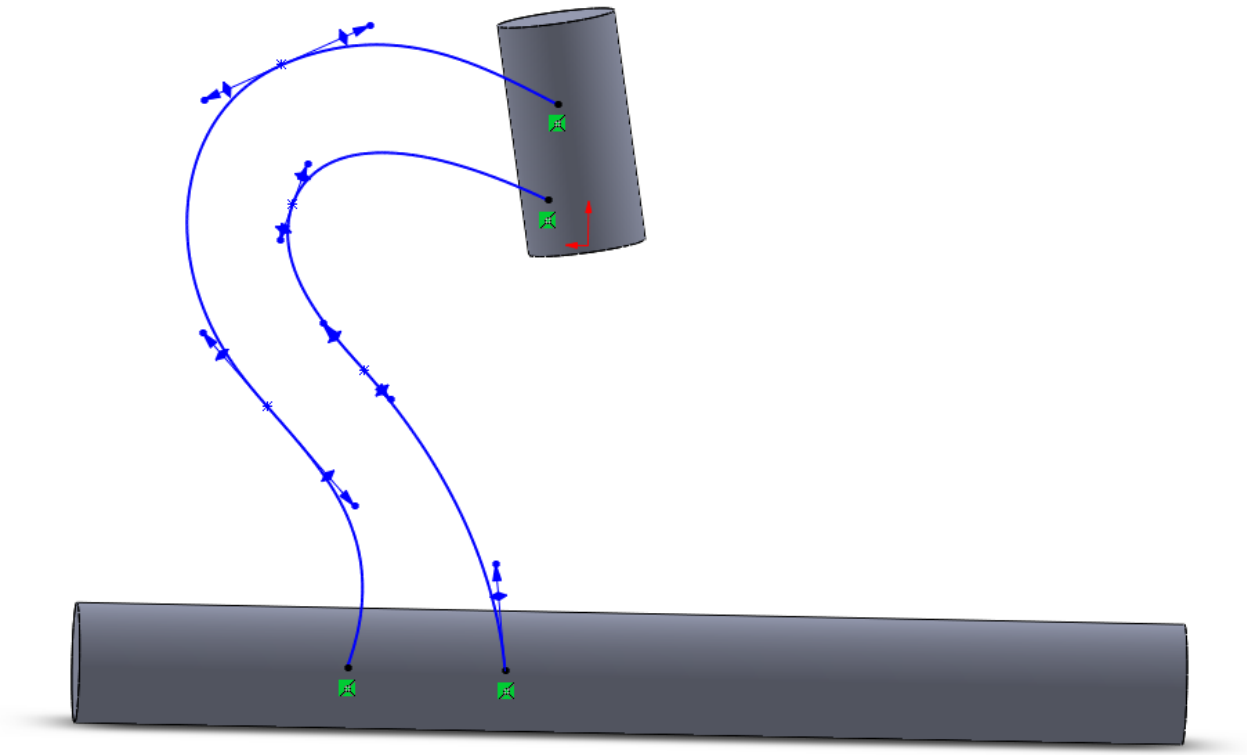

Figure 2.7 HHA Model Spline Customization

2.2.4 Meshing

The 3D meshing for each BT-Shunt was done using ANSYS' built in meshing software, ICEM. More sophisticated meshing software was used at the beginning of this study but was deemed unnecessary due to the relative low complexity of the mesh. Each shunt's mesh was created using body sizing and inflation mesh controls.

First, the body sizing control was set in order to tell the meshing software the largest dimension each face of the mesh can be and set an overall maximum distance between nodes. The entire volume of the geometry was set to a hard-uniform body sizing of 1.5E-4 meters.

Since this study focuses mostly on the interaction of fluid with the wall of the shunt, an inflation mesh was used to make this area more precise for study. The scope of this mesh is set to the entire geometry of the shunt to indicate which object to mesh. Next, the boundaries are set to be the walls

of the geometry (excluding any entrances or exits). To create mesh that is precise near the wall, and less so in the center of the shunt, the inflation was set to a first layer thickness mesh. This allows the first layer of meshing height, the number of layers of inflation there are, and the growth rate between layers to be set. During this study the first layer height was set to 5E-6 meters, the maximum layers was set to 16, and the growth rate left at the default 1.2.

Another important step completed at this time is name selections. Each separate wall is given a descriptive name such that it can be identified and studied later on in the case. These include: IA (innominate artery) velocity input, IA velocity output, aortic vessel, pulmonary artery, shunt wall, shunt wall boundaries 1 & 2, LPA outlet, and RPA outlet (left and right pulmonary artery exits). Figure 2.8 shows the wall groupings of named selections used later in post analysis. It is important to note that the right side of figure is towards the left side of the body, thus the left and right PA outlets seem backwards. An example of the resultant mesh can be seen in Figures 2.9 and 2.10.

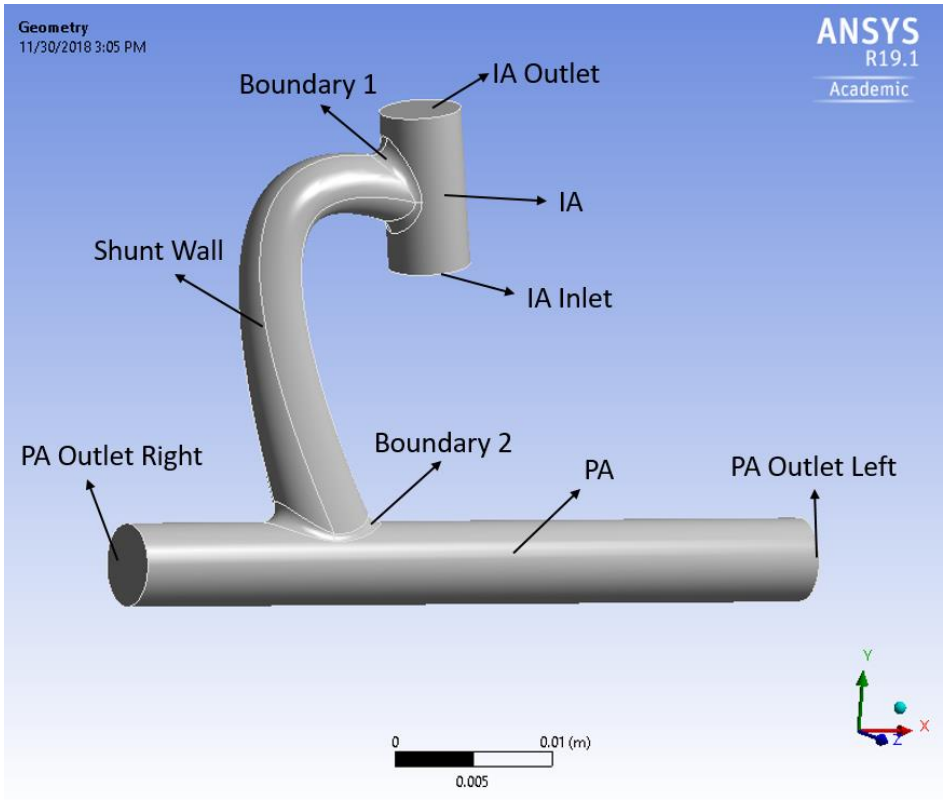

Figure 2.8 BT Shunt Walls - Named Selections

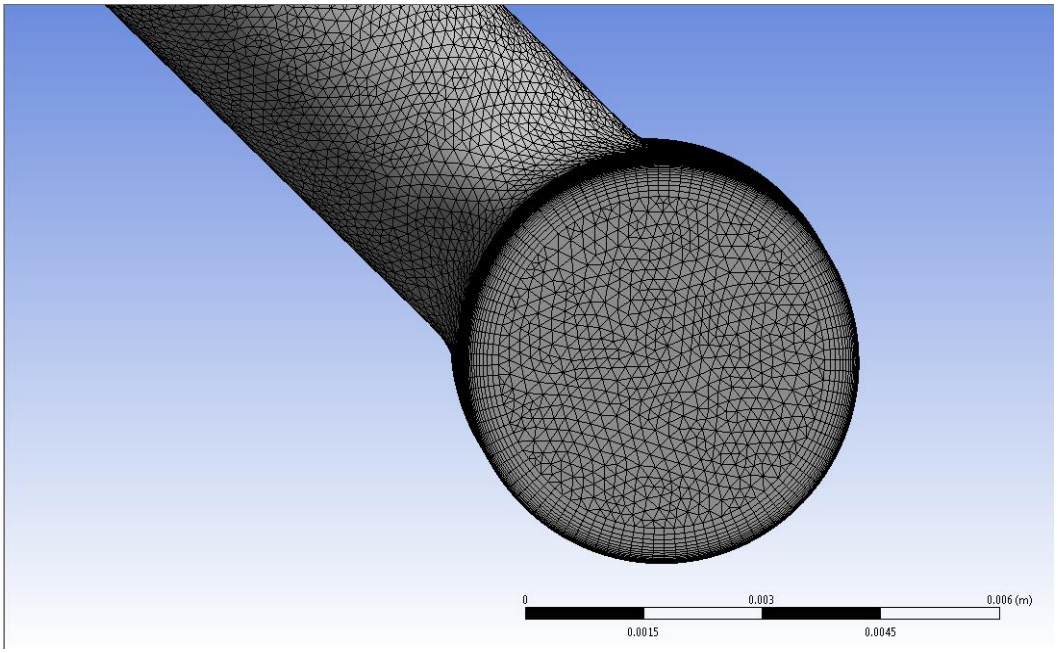

Figure 2.9 Example of Resultant Mesh

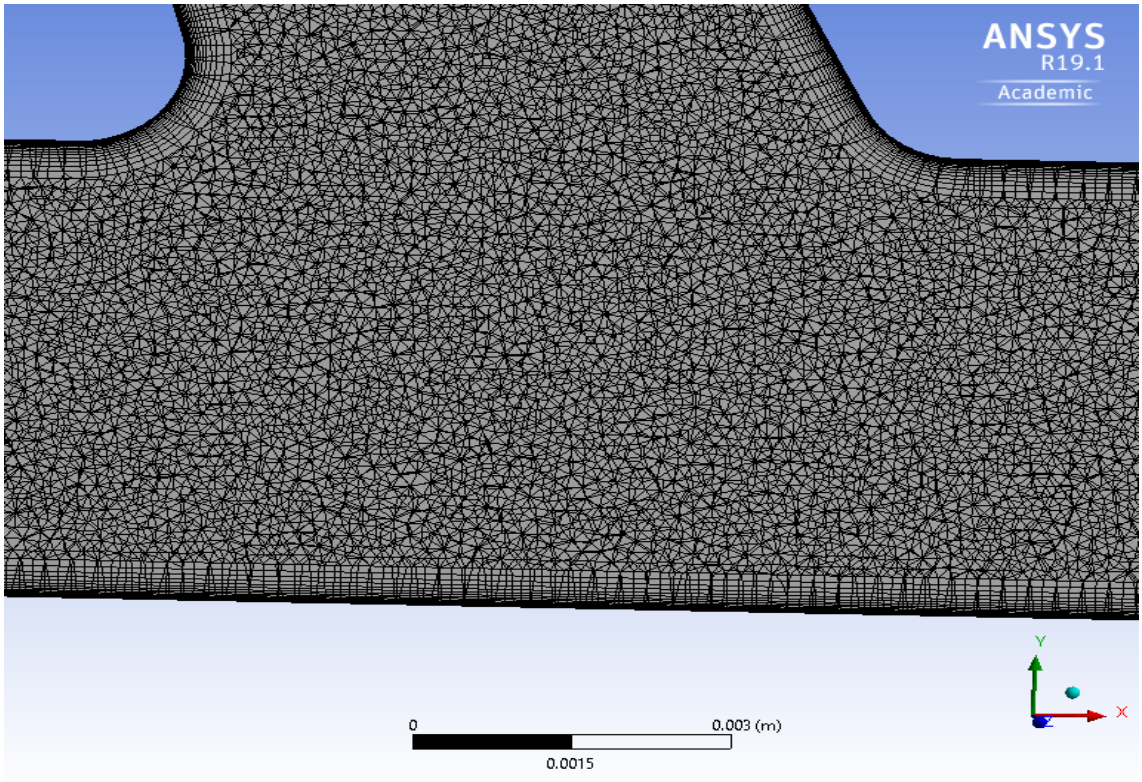

Figure 2.10 Example of Resultant Mesh - Cross Section

2.3 Computational Fluid Dynamics

2.3.1 Overview

CFD or computational fluid dynamics is a subset of fluid mechanics that employs numerical methods and data structures to solve the governing equations of a given fluid flow. CFD is a very powerful tool for analysis and design of fluid systems but requires a computer for the abounding calculations. The basis of many CFD codes is an algorithm for solving the Naiver-Stokes equations which can be simplified by removing various terms or more thoroughly defined by adding terms such as viscous, vorticity, and sub/supersonic flow effects. The most useful advantage of CFD is its ability to solve extremely complex fluid flow problems in relatively short time periods.

Most approaches to CFD are generally done in three phases: pre-processing, simulation, and post-processing. During pre-processing the geometry of the system is defined by importing a predefined CAD file where the physical bonds can be cleaned up and the fluid domain can be extracted. This geometry is then divided into discrete cells called the mesh. The mesh can be set up in nearly infinite sequences, uniform or non-uniform, but typically containing a combination of geometric elements such as pyramidal or polyhedral cells. The mesh is typically finer in areas of high importance or spaces where more precision is needed.

Next, during the simulation phase, the governing equations of fluid flow are discretized on the generated mesh by utilizing a proper numerical algorithm. The computer then solves these discretized equations for the unknown numerical variables of each cell of the mesh. Each equation has a chosen algorithm which determine the order, path, and method for evaluating each cell and their nodes. Algorithms can be either segregated, where momentum equations and pressure corrections are solved separately, or coupled, where both equations are solved simultaneously which is more unstable, uses more CPU, and will converge much slower but provides higher accuracy. The final step, post-processing, is where the data calculated in the simulation is interpreted, illustrated, and used for design analysis and improvement.

2.3.2 Governing Equations

In order to describe fluid flow, three partial differential equations are used to constrain the solution to the laws of the physics: the conservation of mass (continuity equation), the conservation of momentum, and the conservation of energy. When the flow is turbulent additional transport equations are also solved. These equations can be written as [8]:

Continuity equation:

$$\frac{\partial \rho}{\partial t} + \frac{\partial}{\partial x_i}(\rho u_i) = 0 \tag{2-1}$$

Momentum equation:

$$\frac{\partial}{\partial t}(\rho u_i) + \frac{\partial}{\partial x_i}(\rho u_i u_j) = -\frac{\partial p}{\partial x_i} + \frac{\partial \tau_{ij}}{\partial x_i} \tag{2-2}$$

Energy equation:

$$\frac{\partial}{\partial t}\left[\rho\left(h + \frac{1}{2}{u_i}^2\right)\right] + \frac{\partial}{\partial x_i}\left[\rho u_j\left(h + \frac{1}{2}{u_i}^2\right)\right] = \frac{\partial p}{\partial t} + \frac{\partial}{\partial x_j}\left(u_i \tau_{ij} + \lambda \frac{\partial T}{\partial x_j}\right) \tag{2-3}$$

where τ_{ij} the stress tensor and h the enthalpy are formulated as:

$$\tau_{ij} = \mu\left(\frac{\partial u_i}{\partial x_j} + \frac{\partial u_j}{\partial x_i}\right) - \frac{2}{3}\mu \frac{\partial u_i}{\partial x_i}\delta_{ij} \tag{2-4}$$

$$h = C_p T \tag{2-5}$$

The governing equations are solved as a coupled system of five non-linear partial differential equations with six unknown flow-field variables u, v, w, p, ρ, and T. Another equation relating temperature, pressure, and density is provided by the equation of state of the given fluid allowing for a solution.

2.3.3 Turbulence Models

Turbulent flow is defined as any fluid motion characterized by chaotic changes in pressure or flow velocity [9]. While most of the flows in the real world can be considered as turbulent flows, many consist of a combination of laminar, or steady flow, and turbulent flows. The onset of turbulence can be predicted though the use of the dimensionless constant, the Reynolds number. The small fluctuations in velocity, pressure, and temperature fields in turbulent result in changes within transport quantities such as the momentum and energy of the system.

Since these small fluctuations in turbulent can become increasingly expensive and difficult to model due to their unpredictable chaotic nature, manipulations must be made to the governing equations to create a less computationally intensive problem. The governing equations can be simplified or modified in several ways, typically being time-averaged. Turbulence models are used to provide equations to solve for the new unknown variables introduced to simplify the problem or lower computational stress in terms of known values. However, no single turbulence model is universally accepted or superior in all cases of fluid flow and therefore various types of models available depending on the fluid problem and its level of turbulence.

The k-kl-ω transition model, used in this dissertation, is used to predict the onset of transition in boundary layer flow. This model can be used effectively to predict the transition of boundary layer flow from laminar to turbulent regime [10]. However, the K-kl-ω transition model is only applicable with incompressible flow with lower Reynolds numbers not moving far into the turbulent regime. It is a three-equation eddy-viscosity type turbulence model where the three transport equations for turbulent kinetic energy ($\boldsymbol{k_T}$), laminar kinetic energy ($\boldsymbol{k_L}$) and inverse turbulence time scale ($\boldsymbol{\omega}$) are given as:

$$\frac{Dk_T}{Dt} = P_{k_T} + R + R_{NAT} - \omega k_T - D_T + \frac{\partial}{\partial x_j}\left[\left(\nu + \frac{\propto_T}{\propto_k}\right)\frac{\partial k_T}{\partial x_j}\right] \tag{2-6}$$

$$\frac{Dk_L}{Dt} = P_{k_L} + R + R_{NAT} - D_L + \frac{\partial}{\partial x_j}\left[\nu\frac{\partial k_L}{\partial x_j}\right] \tag{2-7}$$

$$\frac{D\omega}{Dt} = C_{\omega 1}\frac{\omega}{k_T}P_{k_T} + \left(\frac{C_{\omega R}}{f_W} - 1\right)\frac{\omega}{k_T}(R + R_{NAT}) - C_{\omega 2}\omega^2 + C_{\omega 3}f_\omega \alpha_T f_W^2\frac{\sqrt{k_T}}{d^3} + \frac{\partial}{\partial x_j}\left[\left(\nu + \frac{\propto_T}{\propto_k}\right)\frac{\partial \omega}{\partial x_j}\right] \tag{2-8}$$

The turbulent and laminar fluctuations corrections are included in the mean flow and energy equations by the eddy viscosity and total thermal diffusivity which are given as:

$$\overline{-u_i u_j} = \nu_{TOT}\left(\frac{\partial U_i}{\partial x_j} + \frac{\partial U_j}{\partial x_i}\right) - \frac{2}{3}k_{TOT}\delta_{ij} \tag{2-9}$$

$$\overline{-u_i \theta} = \alpha_{\theta,TOT}\frac{\partial \theta}{\partial x_i} \tag{2-10}$$

The effective length is characterized as:

$$\lambda_{eff} = MIN(C_\lambda d,\ \lambda_T) \tag{2-11}$$

where $\boldsymbol{\lambda_T}$ is the turbulent length scale and is defined by:

$$\boldsymbol{\lambda_T = \frac{\sqrt{k}}{\omega}} \tag{2-12}$$

with the small-scale energy is defined by:

$$\boldsymbol{k_{T,s} = f_{ss} f_W k_T} \tag{2-13}$$

$$\boldsymbol{f_W = \frac{\lambda_{eff}}{\lambda_T}} \tag{2-14}$$

$$\boldsymbol{f_{ss} = exp\left[-\left(\frac{C_{ss} v \Omega}{k_T}\right)^2\right]} \tag{2-15}$$

The large-scale energy is given by:

$$\boldsymbol{k_{T,l} = k_T - k_{T,s}} \tag{2-16}$$

The turbulence production term generated by turbulent fluctuations is defined as:

$$\boldsymbol{P_{k_T} = v_{T,s} S^2} \tag{2-17}$$

where $\boldsymbol{v_{T,s}}$ is the small-scale turbulent viscosity given as:

$$\boldsymbol{v_{T,s} = f_v f_{INT} C_\mu \sqrt{k_{T,s}} \lambda_{eff}} \tag{2-18}$$

and

$$\boldsymbol{C_\mu = \frac{1}{A_o + A_s (S/\omega)}} \tag{2-19}$$

$$\boldsymbol{f_v = 1 - exp\left(-\frac{\sqrt{R_{e_{T,s}}}}{A_v}\right)} \tag{2-20}$$

A damping function defining the turbulence production due to intermittency is given by:

$$\boldsymbol{f_{INT} = MIN\left(\frac{k_L}{C_{INT} k_{TOT}}, 1\right)} \tag{2-21}$$

$$\boldsymbol{R_{e_{T,s}} = \frac{f_W^2 k_T}{v_\omega}} \tag{2-22}$$

Where $\boldsymbol{P_{k_L}}$ is the production of laminar kinetic energy by large scale turbulent fluctuations given by:

$$\boldsymbol{P_{k_L} = v_{T,l} S^2} \tag{2-23}$$

The large-scale turbulent viscosity $\boldsymbol{v_{T,l}}$ is modeled as:

$$\boldsymbol{v_{T,l} = MIN\left\{v^*_{T,l}, \frac{0.5(k_L + k_{T,L})}{s}\right\}} \tag{2-24}$$

where

$$\boldsymbol{v^*_{T,l} = f_{\tau,1} C_{11} \left(\frac{\Omega \lambda_{eff}^2}{v}\right) \sqrt{f_{T,1}} \lambda_{eff} + \beta_{TS} C_{12} \phi_{NAT} d_\Omega^2} \tag{2-25}$$

A full in-depth guide on the turbulence model equations including the model constants can be found in *ANSYS' Fluent 12.0 Theory Guide [8]*.

2.3.4 Discretization Methods

Now that the governing equations and initial conditions are defined the partial differential equations need to be solved. The problem with this is that these governing equations are highly non-linear equations and cannot be solved analytically except for a few amounts of trivial cases. CFD programs modify these equations into discretized form in order to be solved. The goal of discretization is to turn the PDEs into algebraic expressions that are calculable on the mesh for the flow parameters.

The method in which the PDEs are discretized is based whether the governing equation in question is elliptic, parabolic, or hyperbolic. A suitable iterative numerical method such as finite element method (FEM), finite difference method (FDM), or finite volume method (FVM) is chosen to best discretize the PDE in an algebraic form. In this dissertation as well as most CFD applications, the FVM is employed.

Similar to FEM and FDM, FVM discretizes and solves at individual places within the meshed geometry. FVM, as the name implies, uses a small volume around each node point creating volume integrals and later on surface integrals through the use of the divergence theorem, shown below in Equation (2-26) to represent the various PDEs.

$$\iiint_V (\nabla \cdot \mathbf{F})\, dV = \oiint_S \mathbf{F} \cdot d\mathbf{S} \tag{2-26}$$

These surface integrals are evaluated as flux integrals over the finite volume surface on the mesh. This is very useful in saving processing power, handling memory usage, and quickening solution speed since the methods are conservative; the flux exiting one volume is the same value entering the adjoining volume. In the FVM, the Navier-Stokes equations, conservation of mass, conservation of energy, and turbulence model equations are all discretized and solved on each finite volume in the form below in Equation (2-27).

$$\frac{\partial}{\partial t}\iiint \boldsymbol{Q}\boldsymbol{dV} + \iint \boldsymbol{F}\boldsymbol{dA} = \boldsymbol{0} \tag{2-27}$$

where $\boldsymbol{Q}$ is the vector of conserved variables, $\boldsymbol{F}$ is the flux vector, $\boldsymbol{dV}$ is the volume of the cell, and $\boldsymbol{dA}$ is the surface area of the cell [11].

2.3.5 Solution Methods

In addition to turbulence models and discretization methods, several different solution methods can be chosen within CFD to have greater control over how and in what order the discretization method solves the problem for different variables. These controls include the scheme (segregated or Coupled) and the spatial discretization of: gradients and derivatives, pressure interpolation, momentum, turbulent and laminar kinetic energy, and dissipation rates.

Algorithms can be either segregated, where momentum equations and pressure corrections are solved separately, or coupled, where both equations are solved simultaneously which is more unstable, uses more CPU, and will converge much slower but provides higher accuracy. The coupled algorithm chosen for this dissertation obtains a robust and efficient single-phase implementation for steady-state flows, with superior performance compared to the segregated solution schemes [8].

Within CFD, gradients and derivatives are used for computing scalar values, secondary diffusion terms, and velocity derivatives along the faces of each mesh cell. There are many different gradient solution methods available including: Green-Gauss Cell-Based, Green-Gauss Node-Based, and Least Squares Cell-Based. In this study, the Green-Gauss Node-Based scheme, or GGNB, was chosen due to its increased accuracy compared to standard cell based methods. The node-based approach was first proposed by D. G. Holmes and S. D. Connell who constructed the nodal values to be weighted averages of the surrounding face values [12]. This scheme has high success in unstructured meshes, most importantly triangular and tetrahedral meshes which are used in this dissertation. CGGNB uses the following equation for computing gradients:

$$\boldsymbol{\varphi_f} = \frac{\boldsymbol{1}}{\boldsymbol{N_f}} \sum_{\boldsymbol{n}}^{\boldsymbol{N_f}} \boldsymbol{\varphi_n} \tag{2-28}$$

Where $\boldsymbol{\varphi_f}$ is the gradient of scalar calculated at the face, $\mathbf{N_f}$ is the number of nodes on the face, and $\boldsymbol{\varphi_n}$ is the value calculated at each node. Figure 2.11 illustrates this scheme.

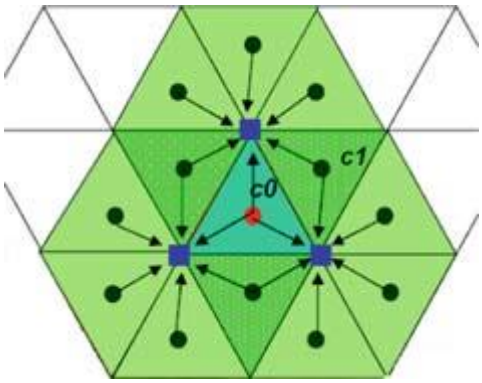

Figure 2.11: Green-Gauss Node-Based Gradient Evaluation Scheme [14]

When using a pressure-based solver, many different pressure interpolation schemes are available to be chosen such as standard, body-force-weighted, PRESTO!, and second-order. These pressure interpolations are used to decide how the pressure gradient term is discretized. In this dissertation the PRESTO! scheme is chosen due to its proficiency with flow through curved domains, high swirl numbers, high-speed rotating flows, and flows with high a Rayleigh number. "This scheme uses the discrete continuity balance for a "staggered" control volume about the face to compute the "staggered" (i.e., face) pressure. This procedure is similar in spirit to the staggered-grid schemes used with structured meshes [8] [13]." PRESTO! avoids interpolation errors and pressure gradient assumptions near the boundaries of the geometry to provide higher accuracy in these areas. A figure depicting the staggering scheme of PRESTO! can be seen in Figure 2.12.

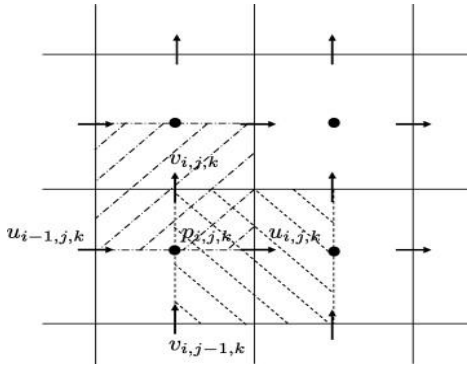

Figure 2.12 PRESTO! Pressure Interpolation Scheme [15]

2.3.6 Description of CFD Solver ANSYS Fluent

In this study the governing equations are solved using Fluent, a commercial CFD program developed by ANSYS Inc. The Fluent software contains the flow modeling capabilities for turbulence, heat transfer, and reactions for industrial and academic applications. The solver is an FVM based software used on a collocated grid [8] with many different numerical schemes available which are customizable based on a given variable including several zero-, one- and two- turbulence models [11]. Fluent is proficient in calculating both compressible and incompressible flows as well as both steady and unsteady flows. Non-Newtonian flows are even available to be modeled. Fluent provides a complete package for a wide range of physical modeling perfect for optimizing many products.

ICEM CFD is a software package that specializes in advanced geometry and mesh generation and can be found in the ANSYS Workbench Suite. It is designed specifically for aerospace, automotive, and electrical engineering problems centered on computational fluid dynamics and structural analysis [16]. ICEM allows uses to create geometries and meshes internally or import geometries and mesh automatically based on mesh controls. The meshing controls allow for various structured, unstructured, or hybrid meshes to be made with their sizing, refinement, inflation, face, and pinch functions. Any type of mesh, simple to complex, can be quickly generated within ICEM making it the perfect partner for ANSYS Fluent.

2.4 Additional Calculations

In order to properly compare different shunt designs after understanding their flows with their respected patient data, each case was resolved with standardized boundary conditions. The same four boundary conditions were given to each of the 3.5 mm shunts (KS, JJ, and DH) and the same for the two 4.0 mm shunts (KC and CS). The standardized values were chosen as a rough average of all boundary conditions for that size shunt. Every optimized HHA shunt model also uses these standardized boundary conditions.

Additional calculations were made with data collected after CFD in Microsoft excel. These were done for completeness and provide more insight into the optimization process by organizing data and provide comparisons between different shunt models. Most of the data collected outside of CFD is dimensional information about the geometry of the model used to record any changes made between subsequent models. This dimensional information could also be used to recreate any model if any file was lost or corrupted.

The first calculation made in excel was the percent difference in flow to the left and right lung. The data points were collected as facet values for volumetric flow rate in m^3/s taken directly from the CFD solution. These were converted to the medical standard of cm^3/min, and the flow rate percent difference between the two exits was calculated for each model.

The other calculation made outside of CFD was a general effective resistance calculation of the model. The effective resistance refers to the cumulated resistance a surface has to the flow of a liquid. Effective resistance is important in a shunt because it determines if the shunt will act similarly to the blood vessel is replacing. Therefore, when creating models, it is important for the effective resistance to stay in a range close to shunts currently in use.

Effective resistance given in units of pascals is determined by several material and shape variables, but since all of our models are of the same material and boundary conditions, the effective resistance is mostly determined by shunt diameter, shunt length, and velocity through the shunt. For our purposes, the effective resistance was estimated to be the major head loss, $\mathbf{h_L}$, in the Dacry-Weisbach Equation (2-29). Since the flow through each shunt fell in the transition zone between laminar and turbulent flows, the Haaland Equation (2-30) was used to find an average friction factor, **f** [17].

$$Effective\ Resistance = \boldsymbol{h_{L_{Major}} = f * \frac{l}{D} * \frac{\rho V^2}{2}} \tag{2-29}$$

$$\boldsymbol{\frac{1}{\sqrt{f}} = -1.8Log[\left(\frac{\frac{\epsilon}{D}}{3.7}\right)^{1.11} + \frac{6.9}{R_e}]} \tag{2-30}$$

Where the effective resistance (pa) is calculated from: **l,** the length of geometry (m), **D**, the diameter (m), **ϱ**, the density of the fluid (kg/m^3), **V**, the velocity of fluid (m/s), **ε**, the geometry's relative roughness (dimensionless), and $\mathbf{R_e}$, the Reynolds number of the flow (dimensionless). The diameter and velocity were taken as averages throughout the entire model.

Chapter 3 Optimization Results for BT Shunt

3.1 Overview

In this chapter the goal of creating an optimized BT shape for lowering the maximum WSS, smoothing the transition between areas of high and low WSS, minimizing flow separation, and equalizing the blood flow to the left (LPA) and right (RPA) pulmonary arteries is started. A new design of shunt could drastically lower the high morbidity rate with BT surgeries by lowering the chance of stenosis, thrombosis, and over shunting.

First, in order to better understand currently used shunts, a study is done to collect data on the fluid properties of four patient designs. These case studies are provided by actual patient specific data and are compared to an initial new shunt design made by Dr. Hoganson. The goal of this first section is to not only provide a basis for future designs to be compared but also pinpoint breakdown areas within the current geometries. These areas will be a focus point on all subsequent optimized models.

Next, the optimization process is begun by creating an all new Solidworks model that is easily customizable. This model is studied with CFD similarly to the case studies and is then modified based on the resulting data. These comparisons are done with blood flow and WSS data along with WSS contour photos, which are all on a scale of 0 to 180 Pa, and velocity profile plots, which are all on a scale of 0 to 2.75 m/s. Discussions with Dr. Hoganson and his team of doctors and engineers are held prior to the creation of a new optimization set. Particular shape changes or problem solutions are discussed and tested in subsequent models.

The final optimized geometry boasted over 120% drop in average WSS at the initial boundary, over 20% drop in overall average WSS, a decline of the maximum WSS by over 25%, and a 19% flow rate difference between the left and right pulmonary exits compared to current shunt models. This model also succeeded to have no symptoms of flow separation with minimal swirling and dead zones. Therefore, this geometry is likely to decrease the likelihood of pulmonary blockage and stenosis occurring within the shunt and is recommended for further testing for clinical practice in thoracic surgery.

3.2 Analysis of Four Case Studies & Initial Design

To begin our study, an analysis of four case studies of current BT shunts was set up to form a basis to compare optimized models to. Dr. Hoganson of Boston Children's Hospital provided the Solidworks file and boundary conditions for the four different models of BT shunt. Each of the boundary conditions and geometries were generated from actual patient data who underwent surgery. These results were not only compared to clinical results of Dr. Hoganson but also a previous study done by Guangyu Bao at Washington University in St. Louis working on a similar project.

Before importing into Fluent, the CAD file for each case study was de-shelled using Solidwork's built in face-delete and knit-surface functions. These altered files were bought into ICEM and meshed utilizing both sizing and inflation functions. Named surfaces are also set so that the boundary conditions can be laid properly in the solver. On average, 5,244,463 cells are created for each model simulation.

For these cases, blood was simulated in Fluent as a Newtonian fluid with a density of 1050 kg/m^3 and viscosity of 0.00255 kg/m s. The walls of each shunt were considered smooth and rigid while the flow was assumed to be fully developed. Each case was given four boundary conditions: inlet and outlet velocity (m/s) of the innominate artery (IA) and outlet pressures (Pa) for both end of the pulmonary artery. Patient data was received in terms of mmHg for pressure, which was converted to Pa, and ml/min for velocity which was converted to m/s using the area of each entrance and exit before being entered into Fluent.

All case studies were computed in a pressure-based CFD solver in Fluent with the turbulence model set to k-kl-omega. A coupled scheme was used to solve pressure and momentum equations simultaneously. PRESTO! pressure interpolation, Green-Gauss Node-Based gradient scheme, and Second-Order upwind schemes for momentum and turbulent kinetic energy were chosen. Each case converged to a residual value of 10^{-6} and continued until 1000 time step iterations was achieved. Several pressure, velocity, and average WSS monitors were set up, recording data every time step to insure proper convergence.

Once each calculation was complete, data was extracted within the solver through the reports tab. Reports for facet average/minimum/maximum WSS as well as volumetric flow rate for both PA exits were taken. All post processing was done in ANSYS CFD Post. Several WSS and velocity contour plots were created for each solved case.

3.2.1 Kaitlyn Staiger's KS Shunt Model

Kaitlyn Staiger's KS shunt model, shown deshelled in Figure 3.1, is a 3.5mm shunt with patient data giving the boundary conditions shown in Table 3.1. Figures 3.2, 3.3, 3.4, and 3.5 illustrate the WSS values within the KS shunt with a scale of 0 to 180 Pa. Finally, Figure 3.6 shows the velocity profile in the middle of the shunt with several cross-sectional profiles at a scale of 0 to 2.75 m/s.

Table 3.1 Patient Data Boundary Conditions for KS Shunt.

#	Boundary	Value	Units
1	IA Velocity Inlet	1303	(ml/min)
2	IA Velocity Outlet	105	(ml/min)
3	RPA Pressure Outlet	15	(mmHg)
4	LPA Pressure Outlet	15	(mmHg)

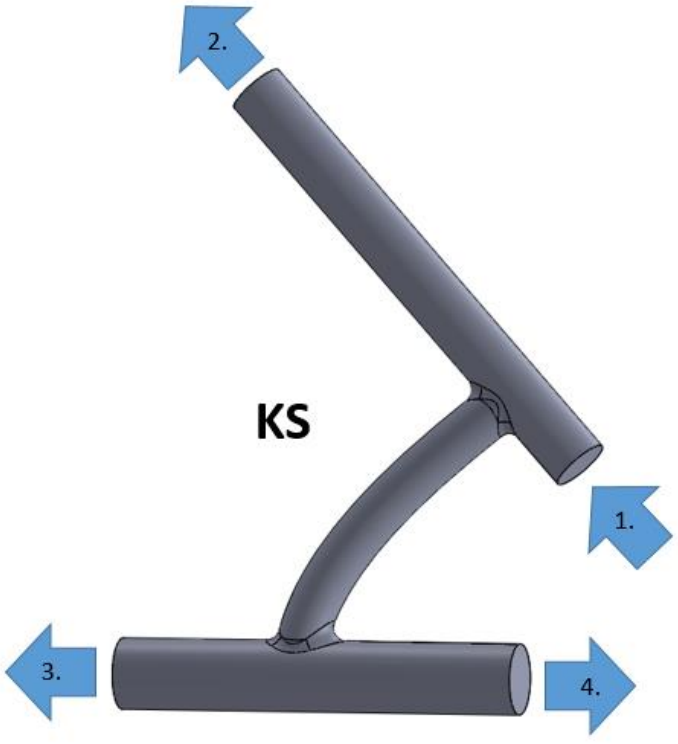

Figure 3.1 De-shelled KS Shunt with Labeled Boundary Conditions

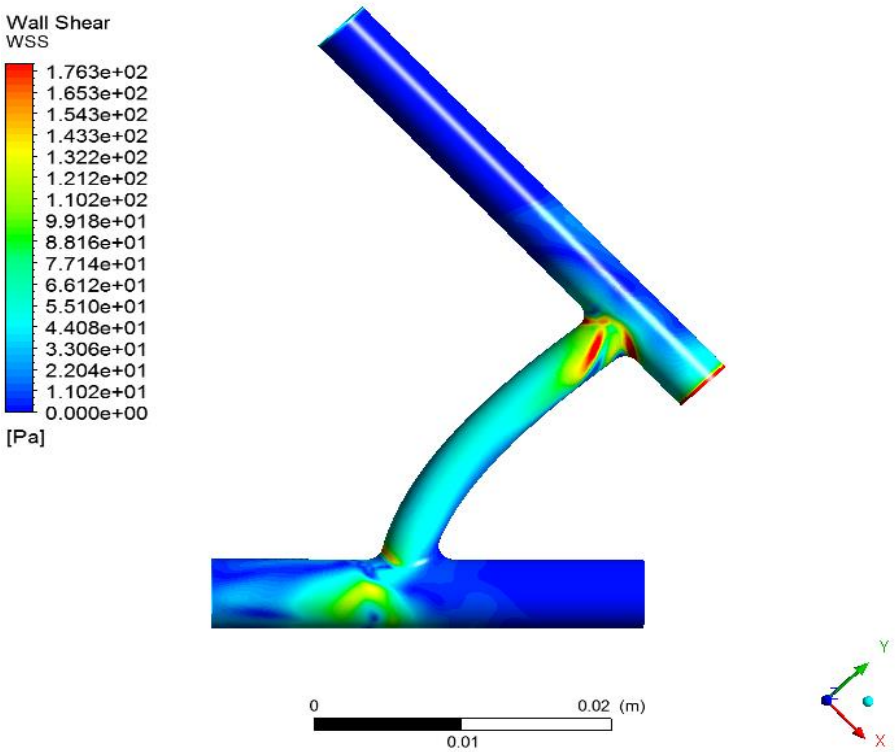

Figure 3.2 Front View WSS Contour of KS Shunt

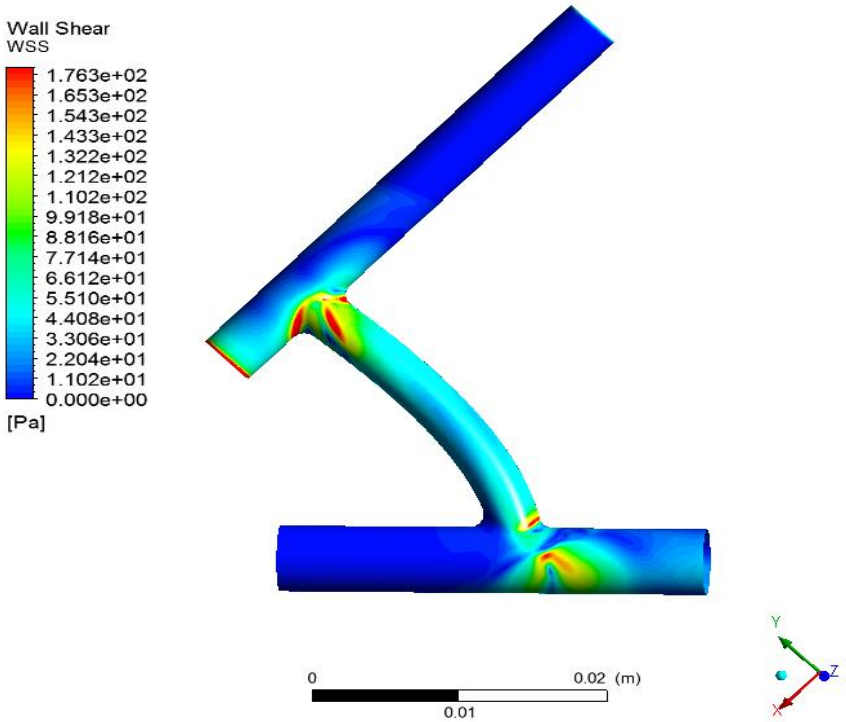

Figure 3.3 Back View WSS Contour of KS Shunt

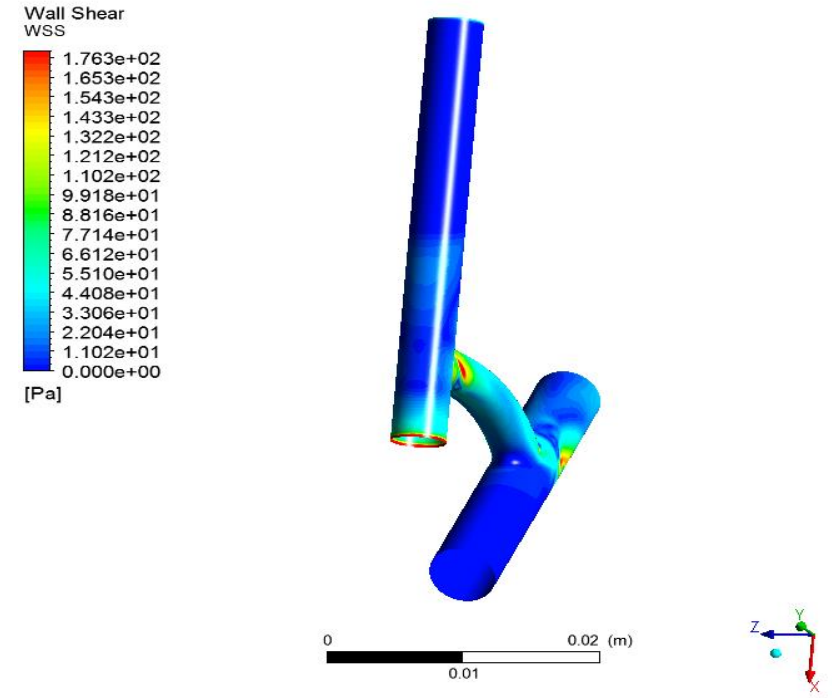

Figure 3.4 Isometric View WSS Contour of KS Shunt

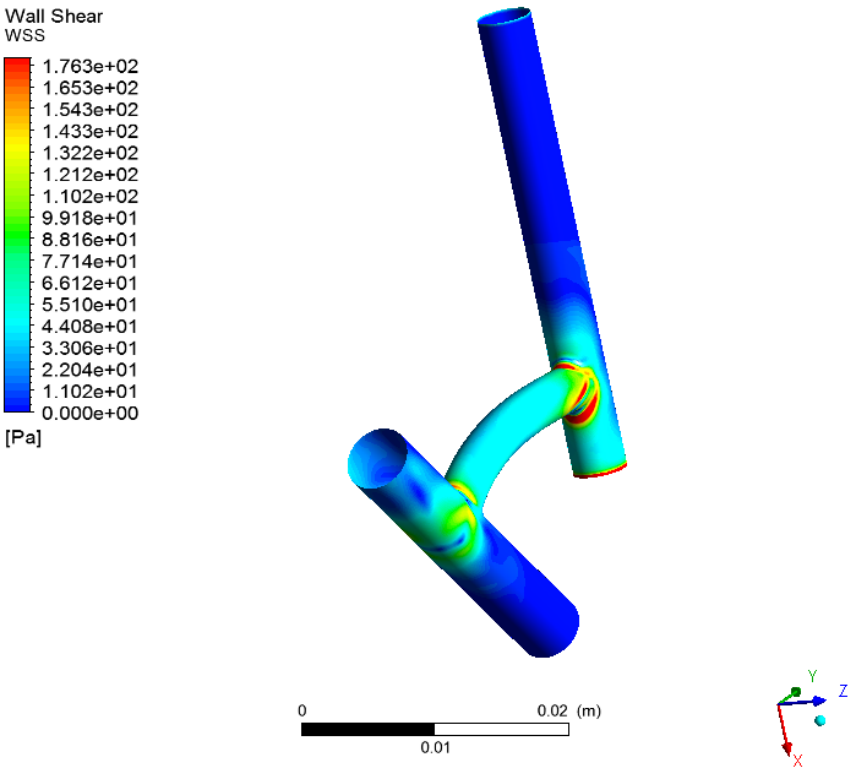

Figure 3.5 Isometric View WSS Contour of KS Shunt

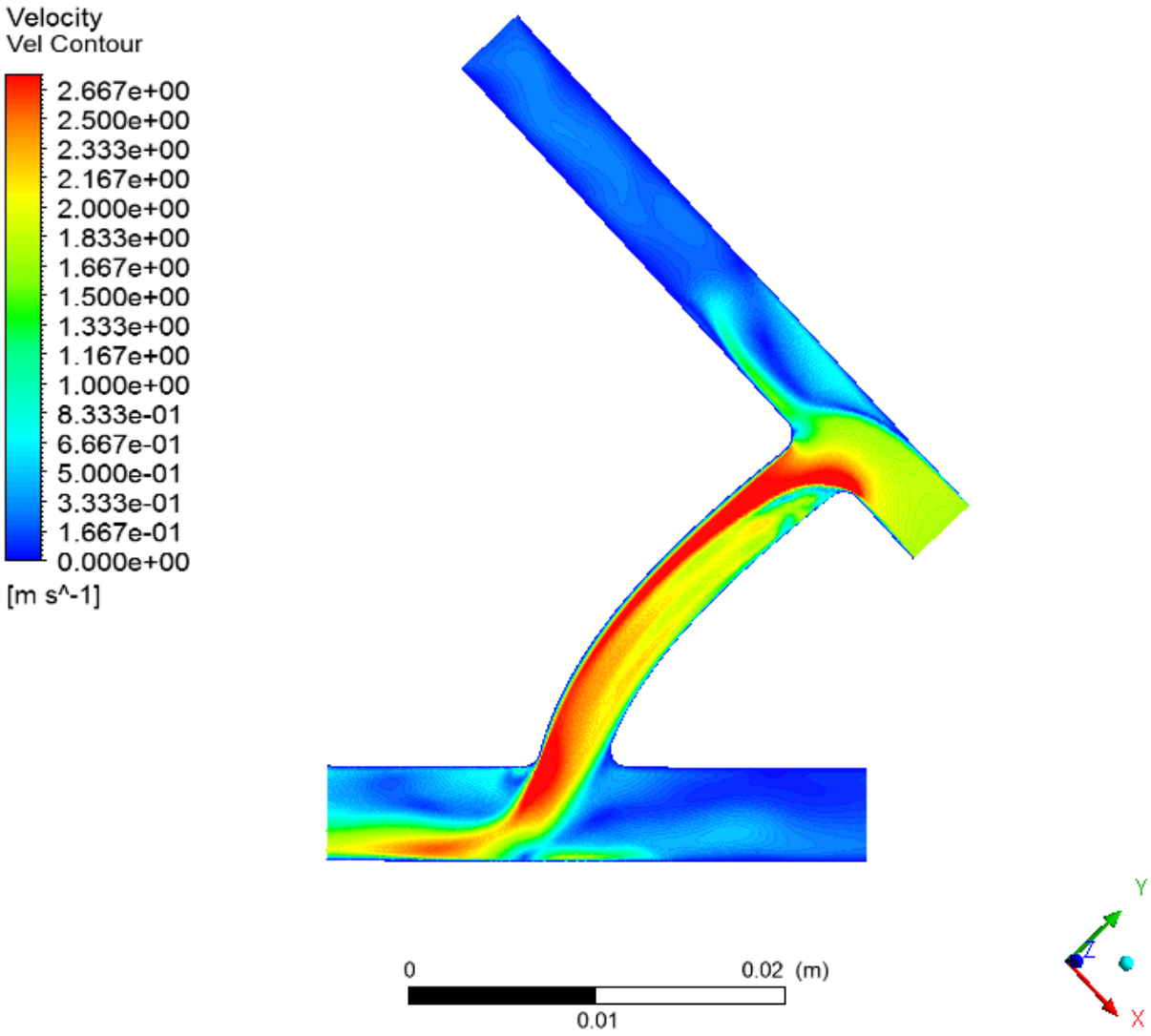

Figure 3.6 Centerline Velocity Contour of KS Shunt

3.2.2 Joanna Jolly's JJ BT Shunt

Joanna Jolly's JJ shunt model, shown deshelled in Figure 3.7, is a 3.5mm shunt with patient data giving the boundary conditions shown in Table 3.2. Figures 3.8, 3.9, 3.10 and 3.11 illustrate the WSS values within the JJ shunt with a scale of 0 to 180 Pa. Finally, Figure 3.12 shows the velocity profile in the middle of the shunt with several cross-sectional profiles at a scale of 0 to 2.75 m/s.

Table 3.2 Patient Data Boundary Conditions for JJ Shunt.

#	Boundary	Value	Units
1	IA Velocity Inlet	1298	(ml/min)
2	IA Velocity Outlet	118	(ml/min)
3	RPA Pressure Outlet	15	(mmHg)
4	LPA Pressure Outlet	15	(mmHg)

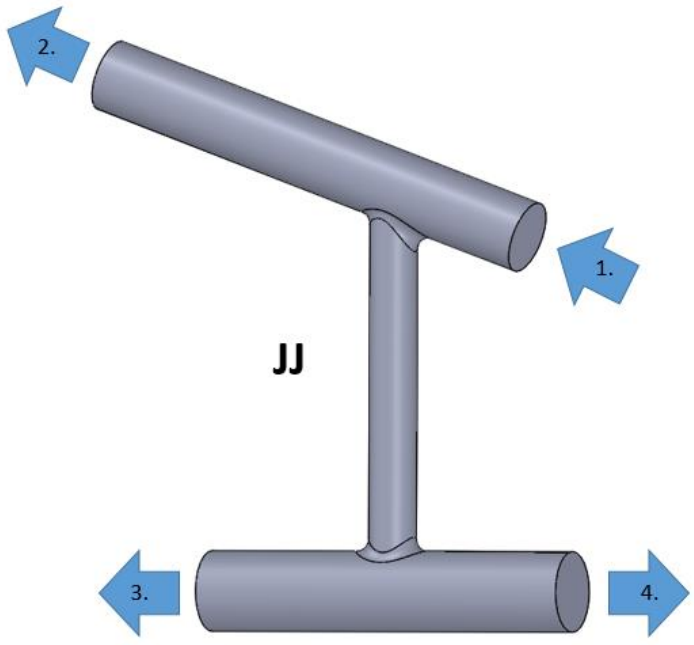

Figure 3.7 De-shelled JJ Shunt with Labeled Boundary Conditions

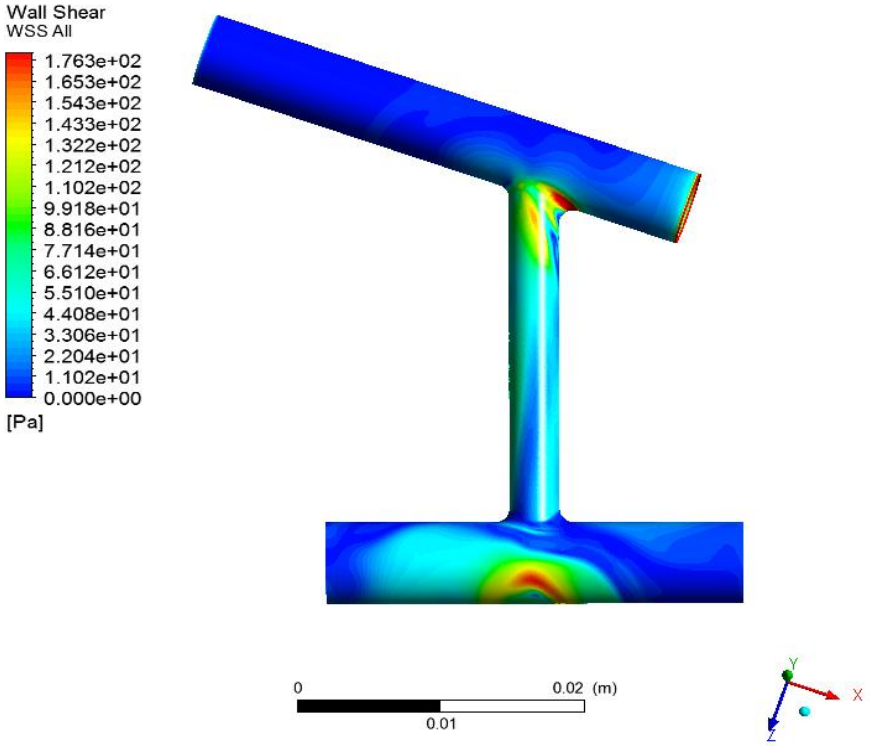

Figure 3.8 Front View WSS Contour of JJ Shunt

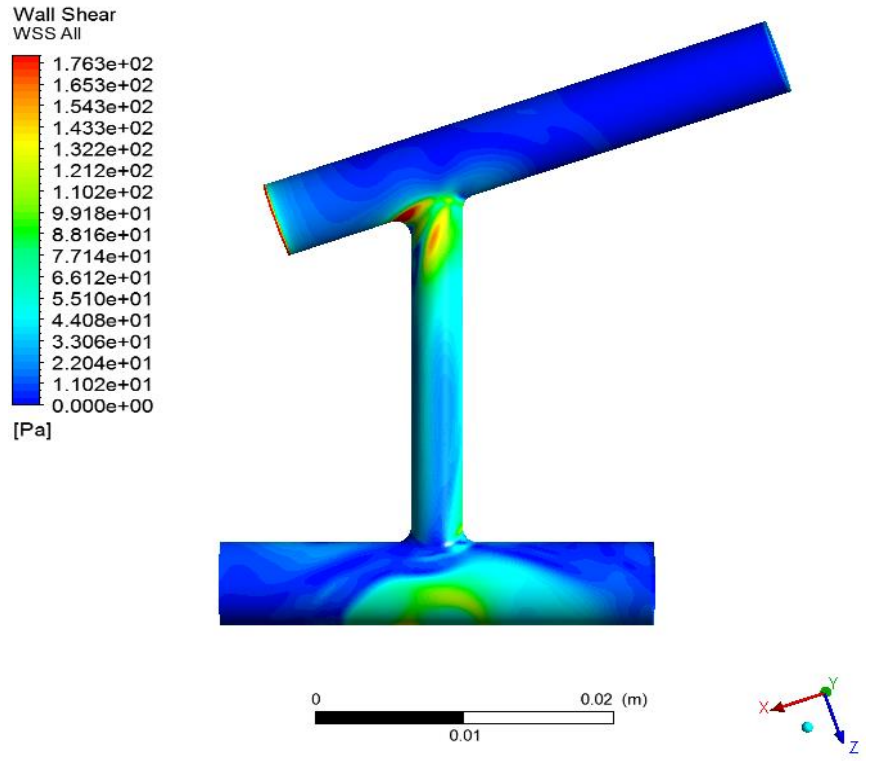

Figure 3.9 Back View WSS Contour of JJ Shunt

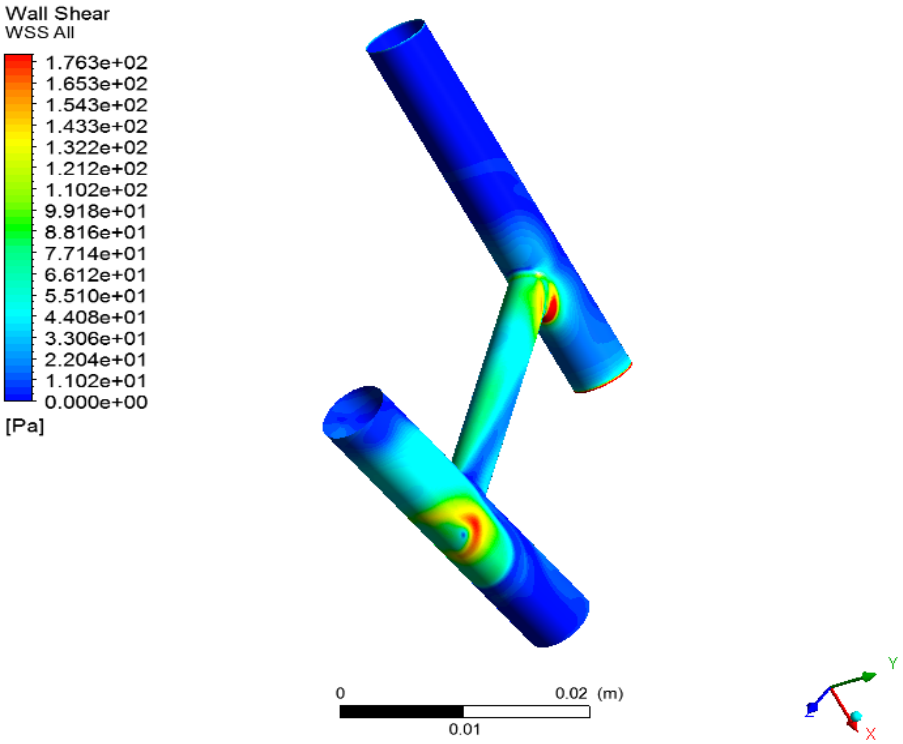

Figure 3.10 Isometric View WSS Contour of JJ Shunt

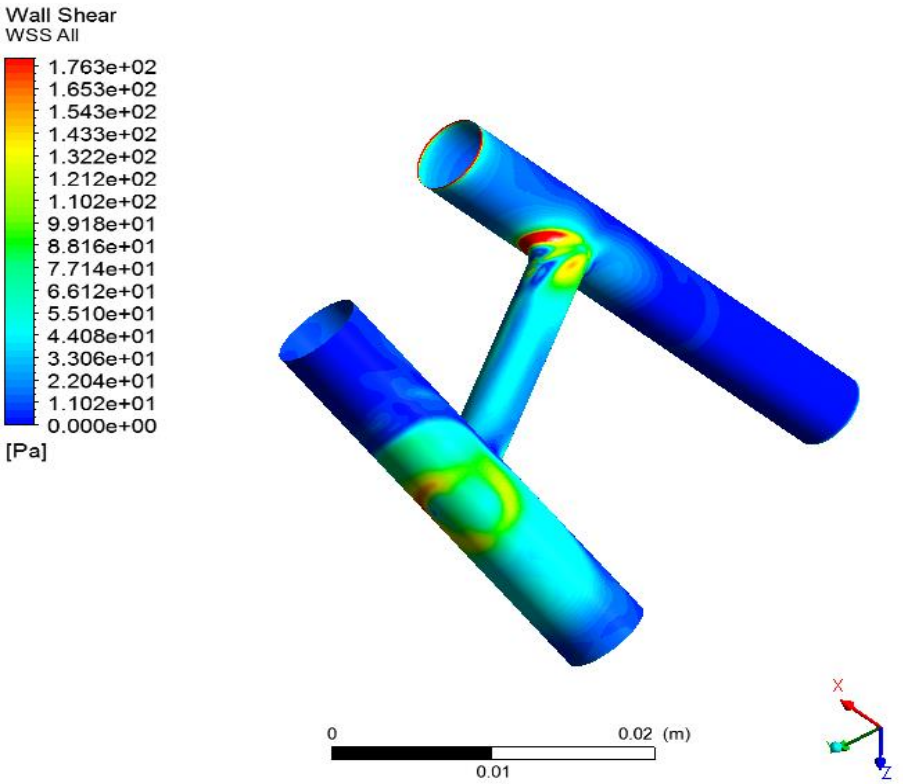

Figure 3.11 Isometric View WSS Contour of JJ Shunt

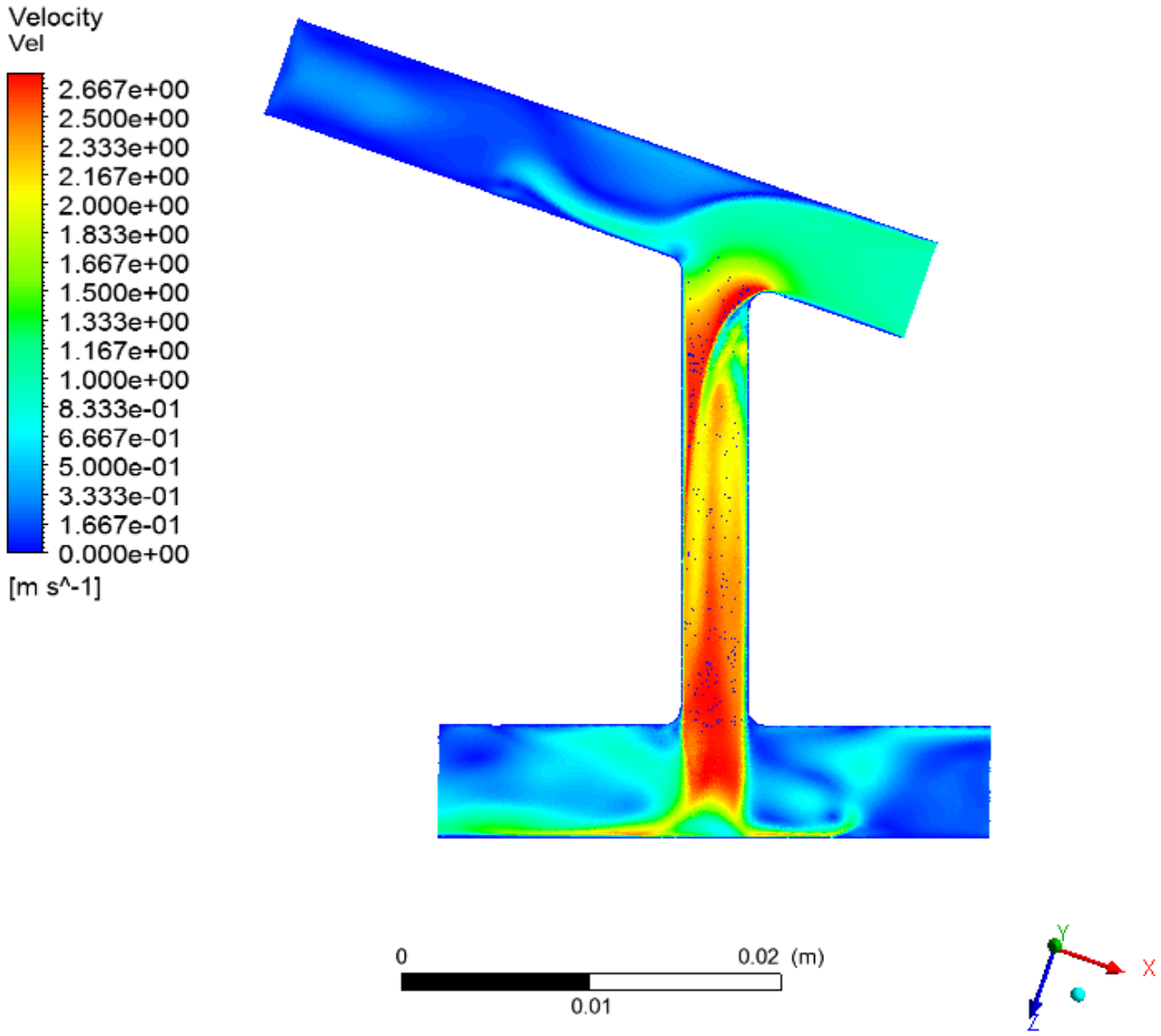

Figure 3.12 Centerline Velocity Contour of JJ Shunt

3.2.3 KC BT Shunt

The KC shunt model, shown deshelled in Figure 3.13, is a 4.0mm shunt with patient data giving the boundary conditions shown in Table 3.3. Figures 3.14, 3.15, 3.16 and 3.17 illustrate the WSS values within the KC shunt with a scale of 0 to 180 Pa. Finally, Figure 3.18 shows the velocity profile in the middle of the shunt with several cross-sectional profiles at a scale of 0 to 2.75 m/s.

Table 3.3 Patient Data Boundary Conditions for KC Shunt.

#	Boundary	Value	Units
1	IA Velocity Inlet	1198	(ml/min)
2	IA Velocity Outlet	128	(ml/min)
3	RPA Pressure Outlet	16	(mmHg)
4	LPA Pressure Outlet	15	(mmHg)

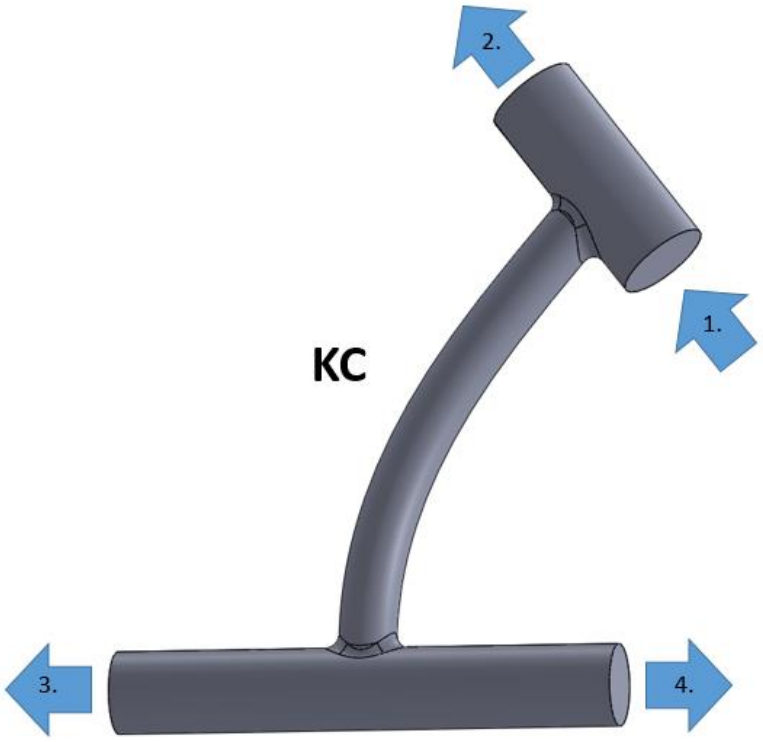

Figure 3.13 De-shelled KC Shunt with Labeled Boundary Conditions

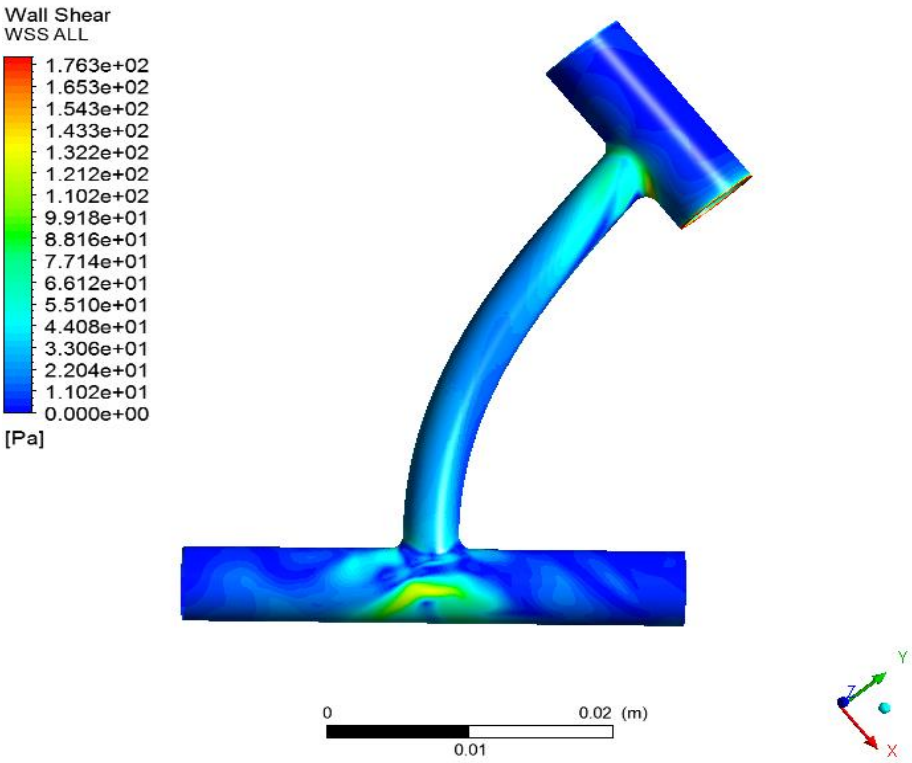

Figure 3.14 Front View WSS Contour of KC Shunt

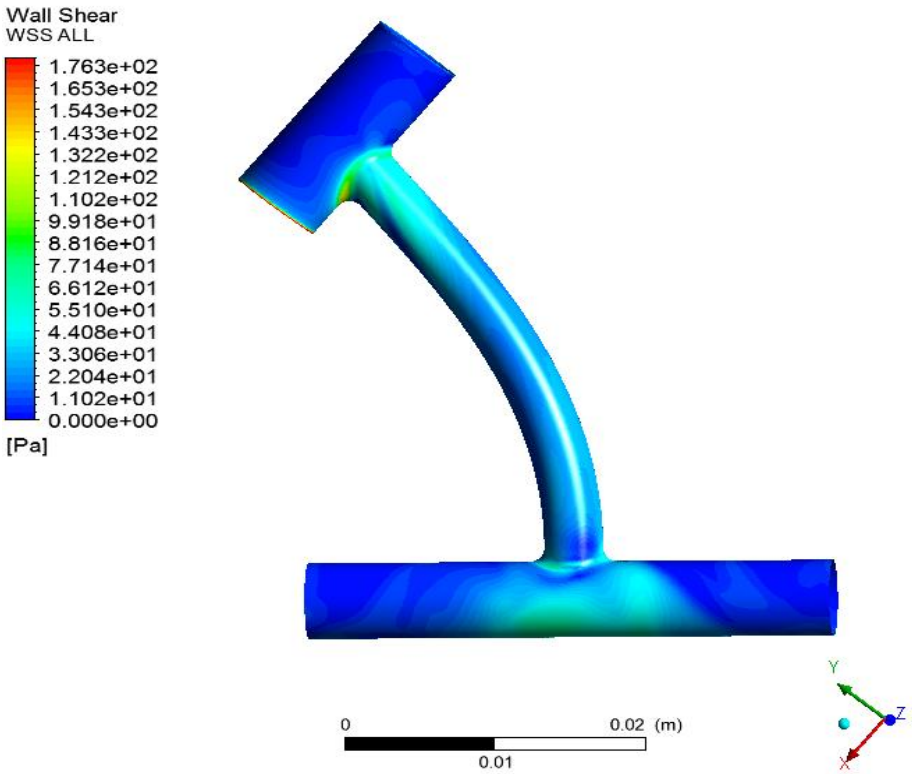

Figure 3.15 Back View WSS Contour of KC Shunt

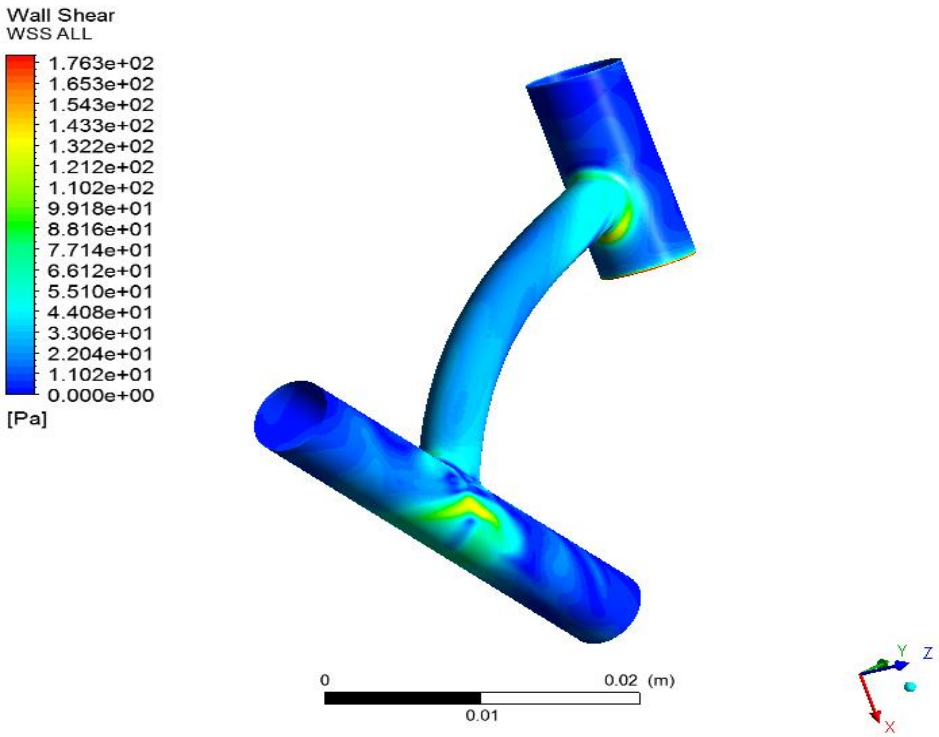

Figure 3.16 Isometric View WSS Contour of KC Shunt

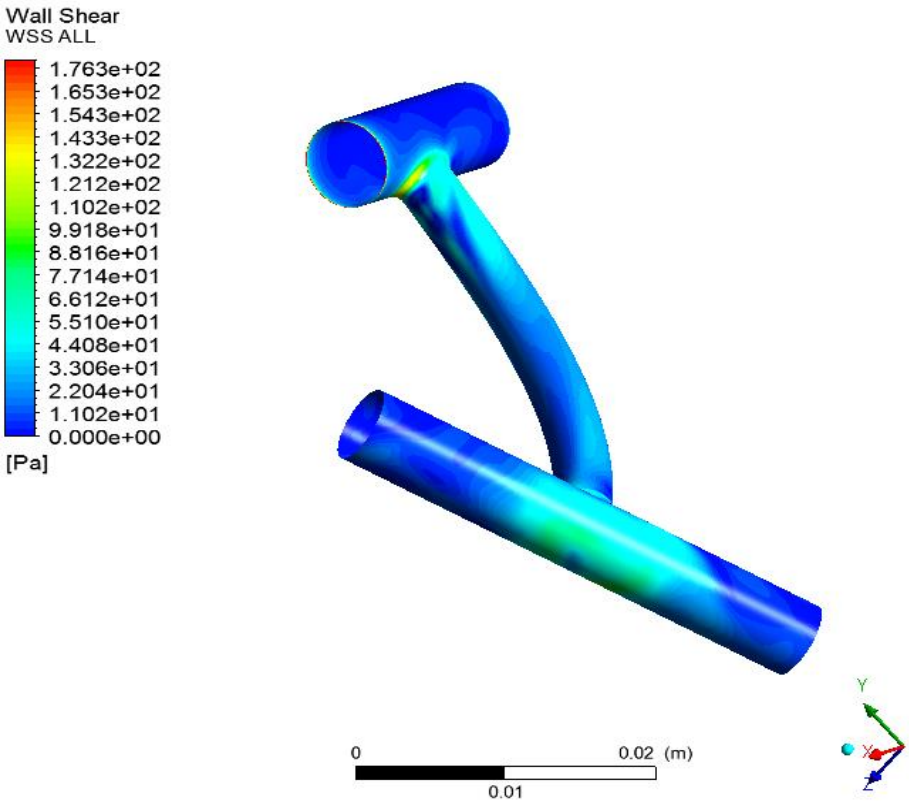

Figure 3.17 Isometric View WSS Contour of KC Shunt

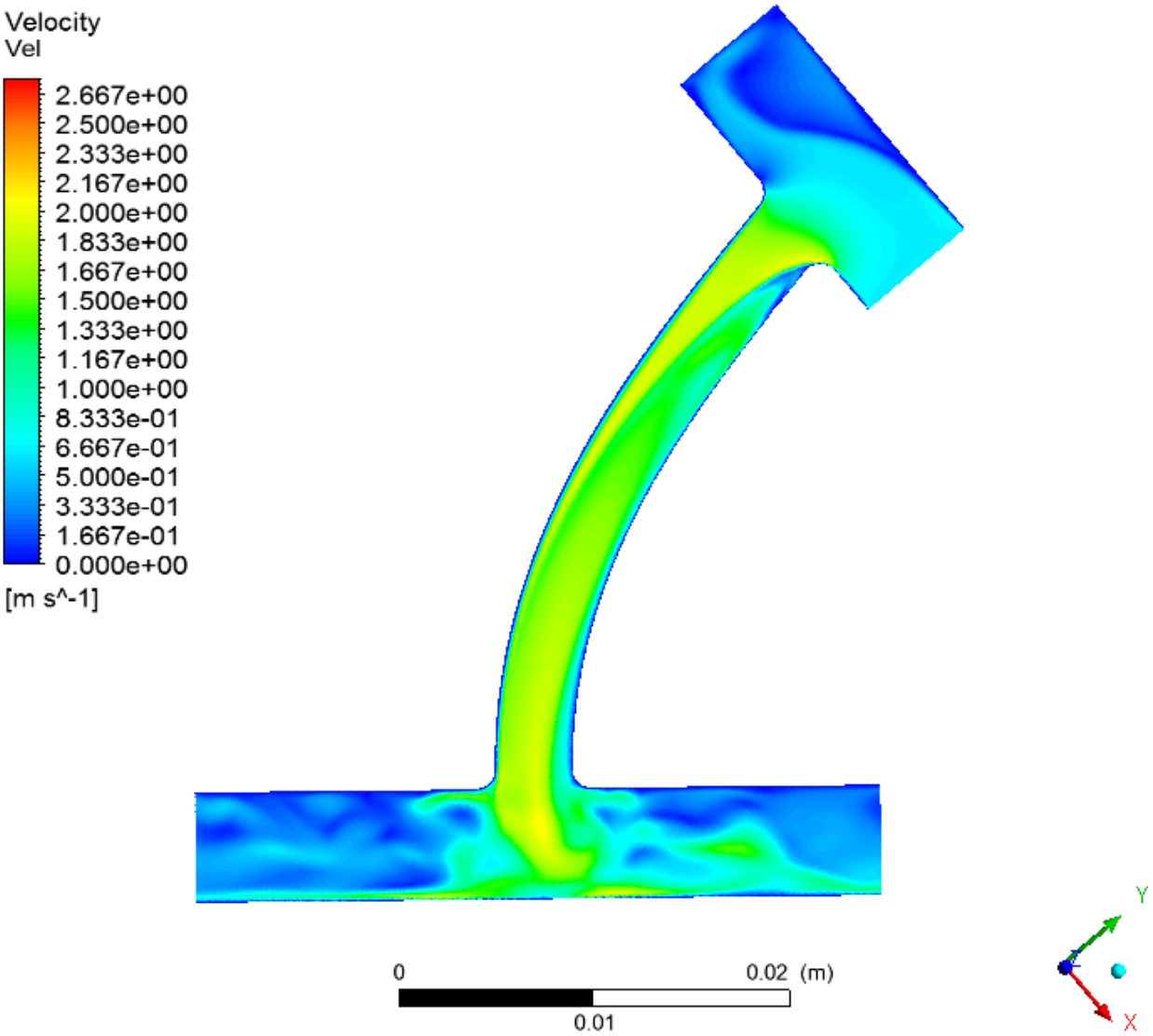

Figure 3.18 Centerline Velocity Contour of KC Shunt

3.2.4 Central Shunt CS BT Shunt

The Central Shunt CS shunt model, shown deshelled in Figure 3.19, is a 3.5mm shunt with patient data giving the boundary conditions shown in Table 3.4. Figures 3.20, 3.21, 3.22 and 3.23 illustrate the WSS values within the KS shunt with a scale of 0 to 180 Pa. Finally, Figure 3.24 shows the velocity profile in the middle of the shunt with several cross-sectional profiles at a scale of 0 to 2.75 m/s.

Table 3.4 Patient Data Boundary Conditions for CS Shunt.

#	Boundary	Value	Units
1	IA Velocity Inlet	1653	(ml/min)
2	IA Velocity Outlet	155	(ml/min)
3	RPA Pressure Outlet	15	(mmHg)
4	LPA Pressure Outlet	15	(mmHg)

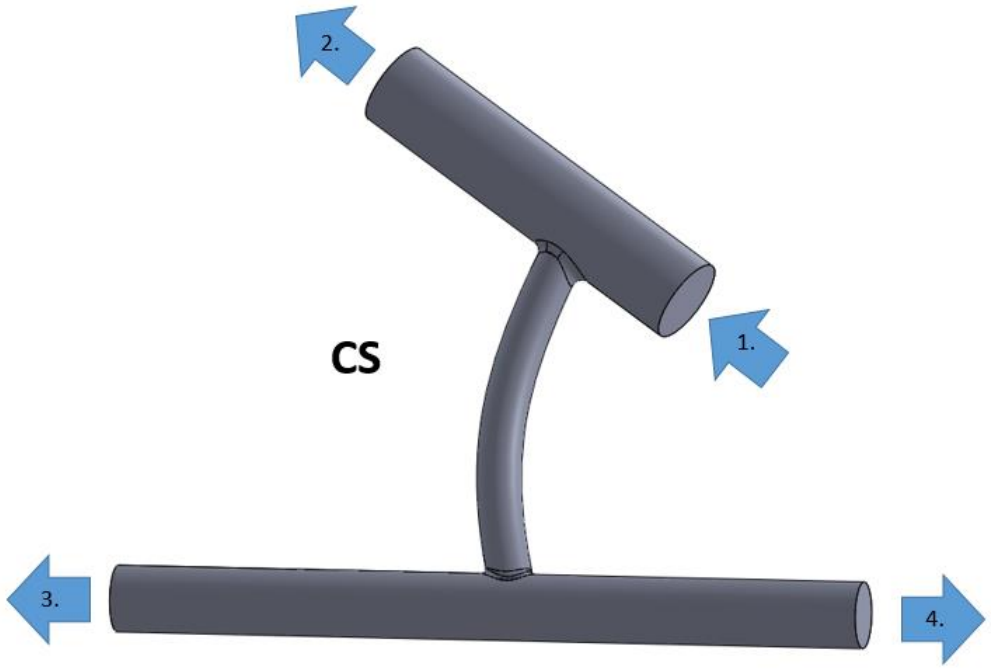

Figure 3.19 De-shelled CS Shunt with Labeled Boundary Conditions

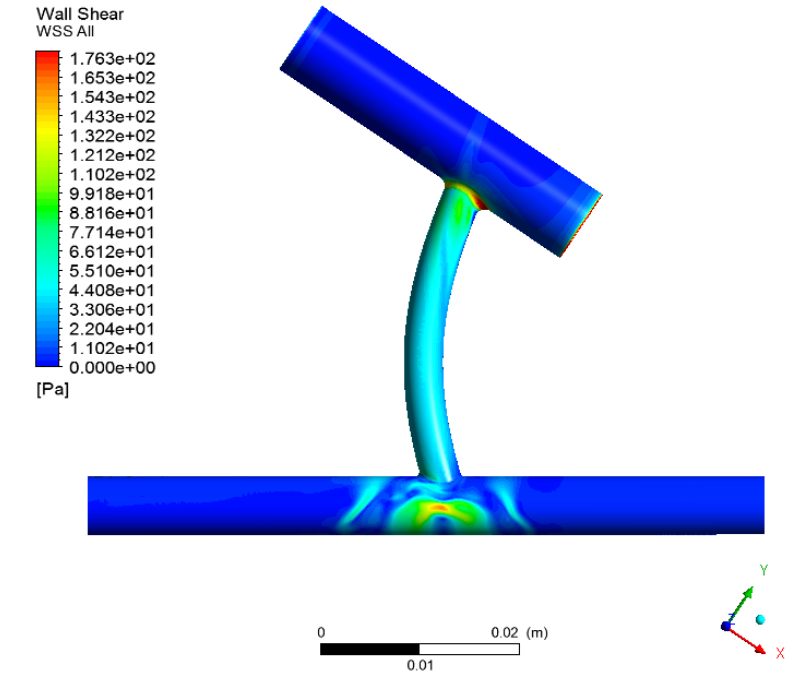

Figure 3.20 Front View WSS Contour of CS Shunt

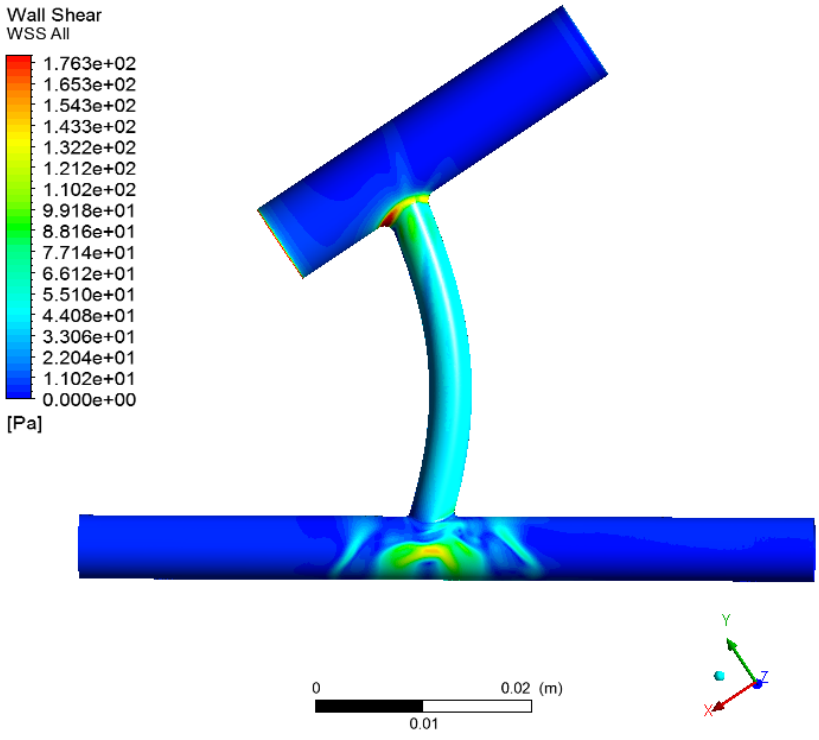

Figure 3.21 Back View WSS Contour of CS Shunt

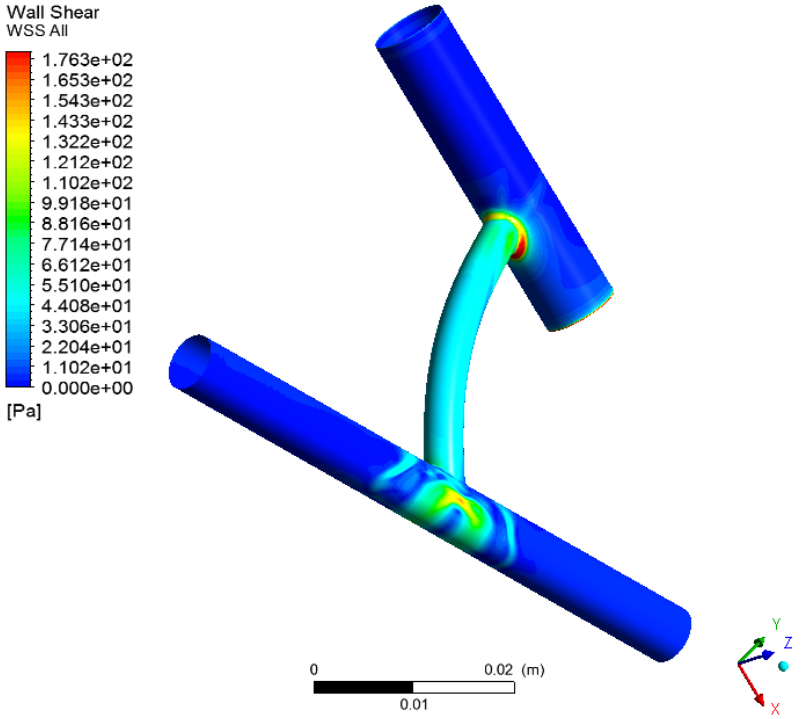

Figure 3.22 Isometric View WSS Contour of CS Shunt

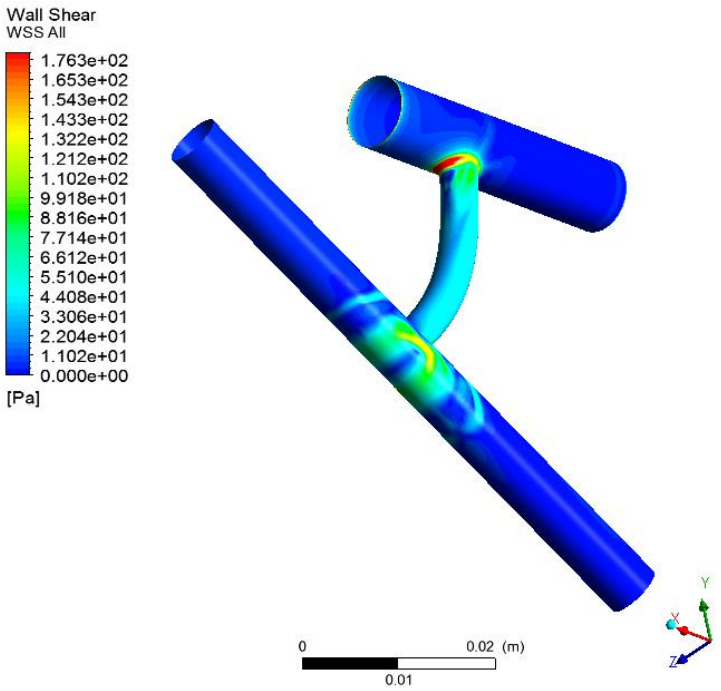

Figure 3.23 Isometric View WSS Contour of CS Shunt

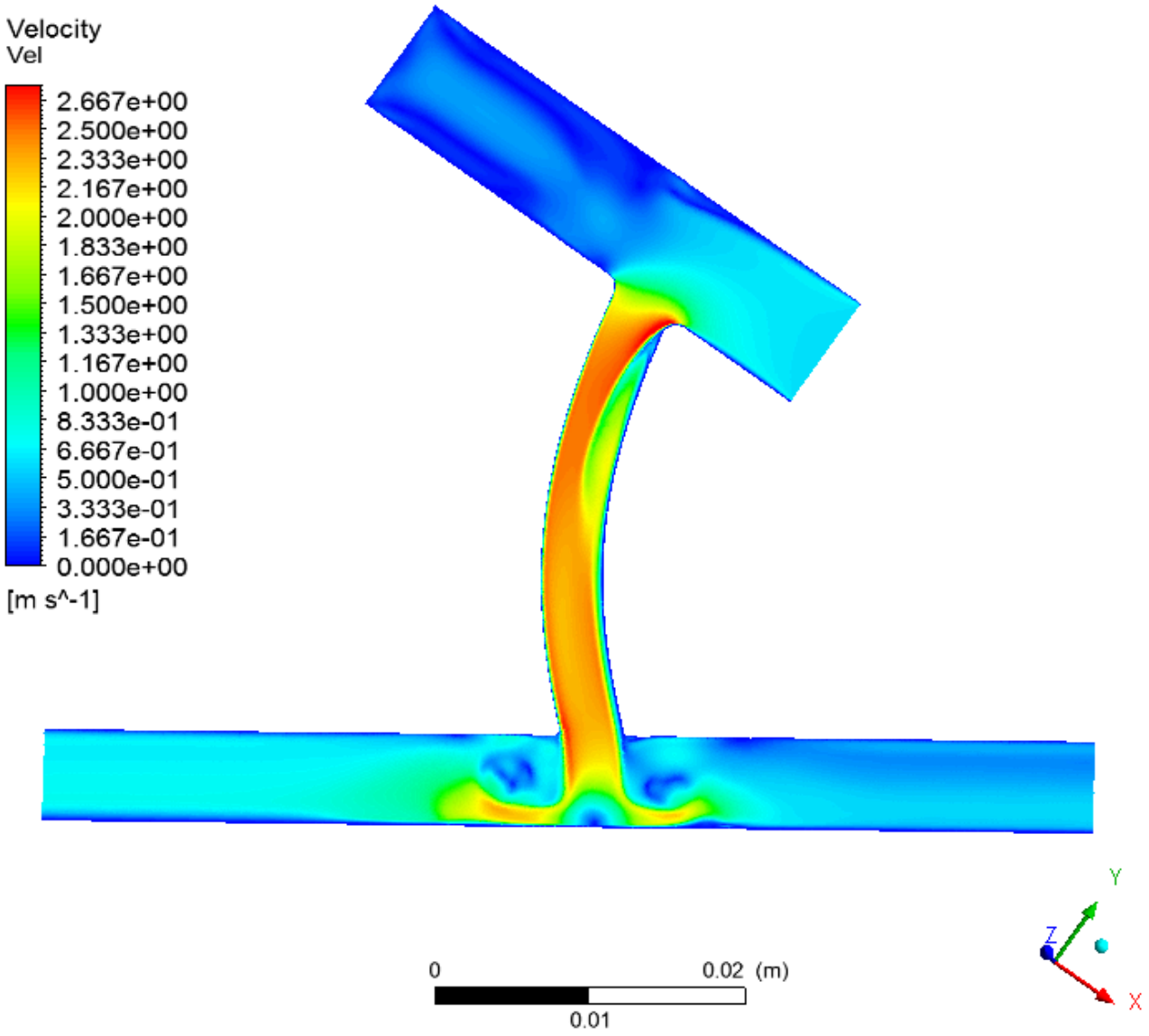

Figure 3.24 Centerline Velocity Contour of BT Shunt

3.2.5 David Hoganson's DH BT Shunt

David Hoganson's original DH shunt model, shown deshelled in Figure 3.25, is a 3.5mm shunt with patient data giving the boundary conditions shown in Table 3.5. The DH shunt has one addition pressure outlet for the PA offshoot in the geometry. Figures 3.26, 3.27, 3.28, and 3.29 illustrate the WSS values within the KS shunt with a scale of 0 to 180 Pa. Finally, Figure 3.30 shows the velocity profile in the middle of the shunt with several cross-sectional profiles at a scale of 0 to 2.75 m/s.

Table 3.5 Patient Data Boundary Conditions for DH Shunt.

#	Boundary	Value	Units
1	IA Velocity Inlet	1054	(ml/min)
2	IA Velocity Outlet	82	(ml/min)
3	RPA Pressure Outlet	14	(mmHg)
4	LPA Pressure Outlet	14	(mmHg)
5	Offshoot Pressure Outlet	14	(mmHg)

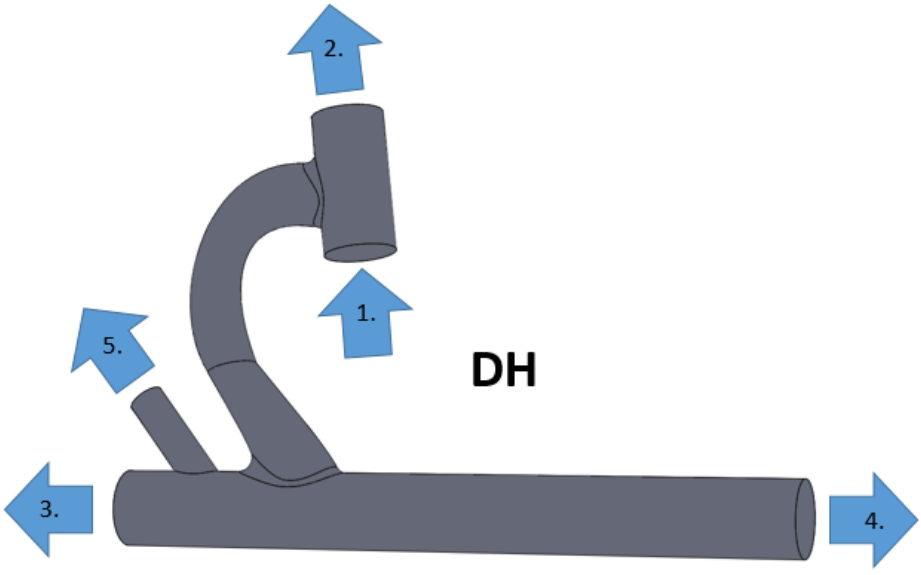

Figure 3.25 **De-shelled DH Shunt with Labeled Boundary Conditions**

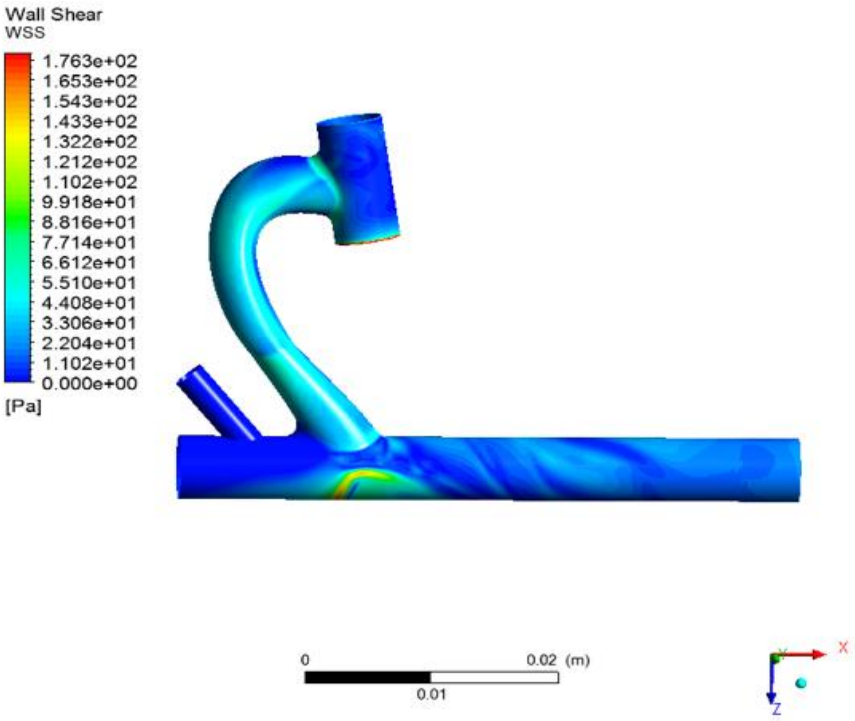

Figure 3.26 Front View WSS Contour of DH Shunt

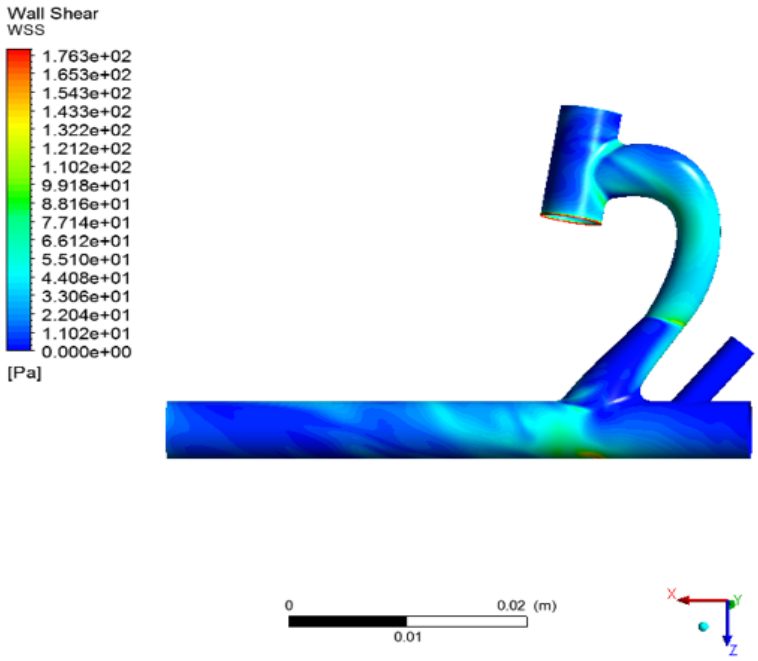

Figure 3.27 Back View WSS Contour of DH Shunt

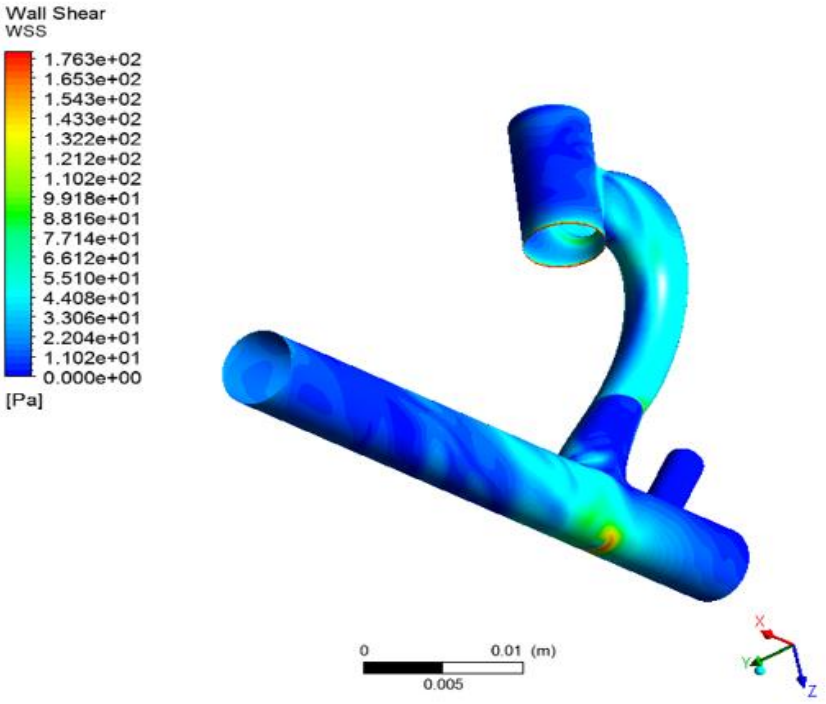

Figure 3.28 Isometric View WSS Contour of DH Shunt

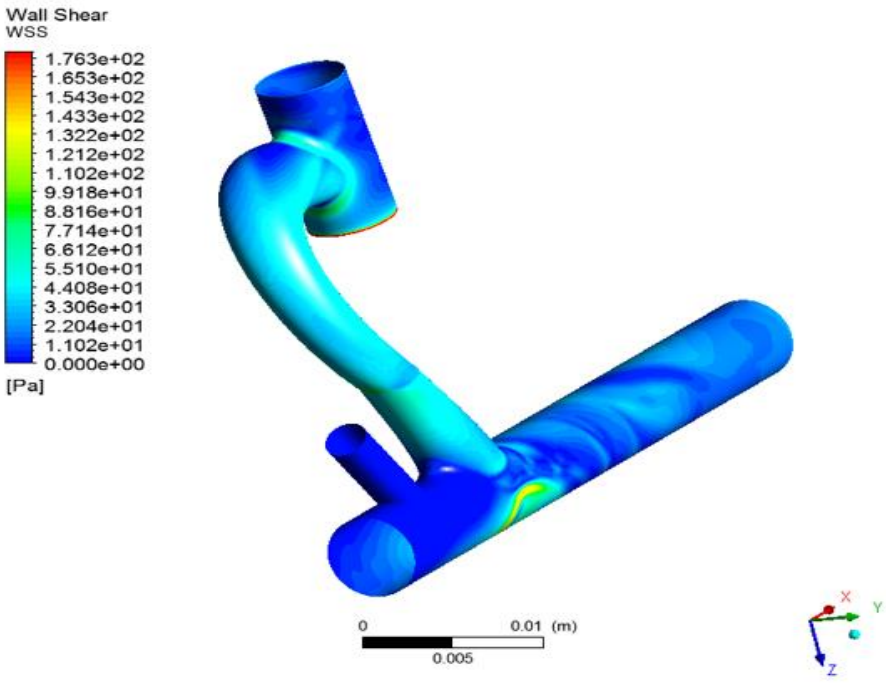

Figure 3.29 Isometric View WSS Contour of DH Shunt

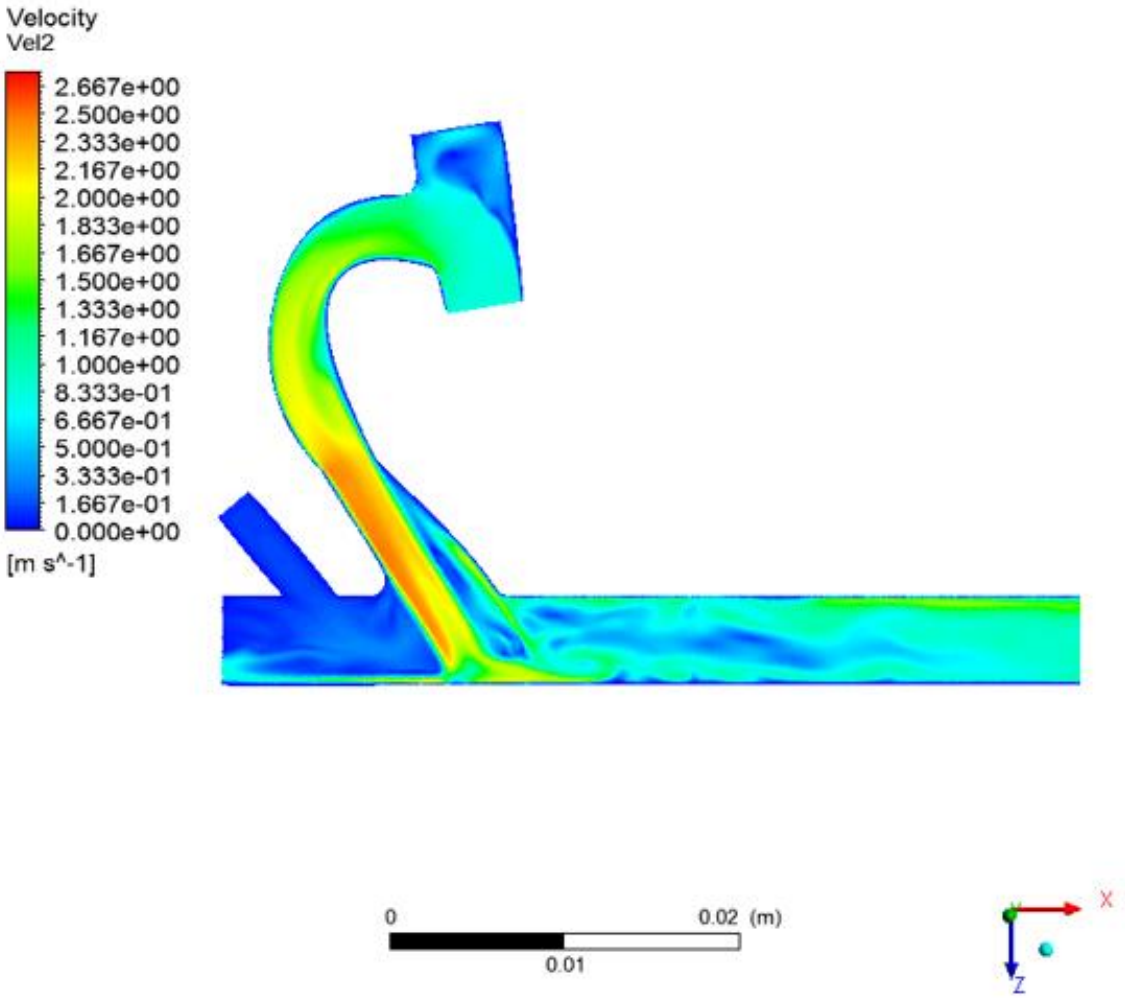

Figure 3.30 Centerline Velocity Contour of BT Shunt

3.2.6 Comparison of the Results of 4 Case Studies & Initial Design

The WSS data for each of the case studies (KS, JJ, KC, and CS) show the importance of fillets for gradual flow transition into the shunt. The KC shunt, the only case study involving a fillet, noticeably has lower WSS stress values around boundary 1 than any other case study and eliminates large WSS spikes found afterwards. In each of the case studies, large flow separation at the onset of boundary 1 can be seen in the velocity contour images. This is remarked by Dr. Hoganson as "the breakdown area" of shunts currently used in surgery being the leading cause of thrombosis. The flow separation creates pockets of dead zone where non-moving flow promotes platelet aggregation or thrombosis where clots are likely to occur due to the lack of WSS.

The initial DH shunt design showed many improvements in this breakdown area by eliminating the flow separation at boundary 1. This is due to the plane angle at which the shunt is connected to the IA and the larger fillet design. The abrupt transition between the two pieces of the DH are proven to be a problem area within both the WSS contour and velocity profile. This is an important area to eliminate when designing the new HHA shunts. The PA offshoot is also proven to be unnecessary to the model due to its non-effect on the solution.

After each case solution, WSS data was imported into excel for the three wall groups: boundary 1 (B1), boundary 2 (B2), and the over shunt wall. Refer to Figure 2.8 for named selection identification. Table 3.6 shows the average/minimum/maximum wall shear stress values at each location for every case study. Table 3.7 shows the estimated effective resistance values of each geometry. These are the basis used for understanding how much WSS and effective resistance is typically found in modern shunts.

Table 3.6 Average/Minimum/Max Wall Shear Values (Pa) for Each Case Study.

WSS (Pa)	AVG			MIN			MAX		
SHUNT	B1	B2	Shunt	B1	B2	Shunt	B1	B2	Shunt
KS	117.835	31.689	51.3689	1.148	0.189	1.013	408.837	253.74	237.713
JJ	104.825	16.556	47.512	0.882	0.642	0.736	302.112	115.64	169.966
KC	67.425	27.449	23.84	0.97	0.409	0.081	167.665	78.497	75.319
CS	120.155	27.155	39.85	1.068	0.24	1.367	269.163	127.79	110.57
DH	44.318	11.929	30.0623	0.447	0.252	0.025	112.593	77.462	141.627

Table 3.7 Estimated Effective Resistance (Pa) for Each Case Study.

SHUNT	Effective Resistance (Pa)
KS	776.8289361
JJ	725.2880576
KC	933.7606367
CS	946.0279012
HHA	764.6245757

Although each case follows different boundary conditions, it is found that a larger diameter shunt will receive lower overall average and maximum WSS values, the DH performs best in both boundary areas. The average WSS of the IA boundary of a 3.5mm shunt is 104-118 Pa, while the introduction of a fillet and greater curvature in the DH shunt lowers this value to 44 Pa. This is also lower than any of the 4.0 mm cases. Most importantly, from this data it found that the standard effective resistance of a BT shunt is estimated to be 700-800 Pa for a 3.5mm shunt and 900-1000 Pa for a 4.0 mm. This will be an important qualification for newly designed shunts.

In order to properly compare the various case study data to one another, standardized boundary conditions were set for the 3.5 mm shunts (KC, JJ, and DH) and 4.0 mm shunts (CS and KC). These values, shown below in Tables 3.7 and 3.8, were an average of all boundary conditions of that shunt size. Table 3.9 shows the average/minimum/maximum WSS values of each area of the shunt under standardized conditions. This is used to identify favorable and negative qualities of each modern day shunt.

Table 3.8 Standardized Boundary Conditions for 3.5 mm Shunts KC, JJ, and DH

#	Boundary	Value	Units
1	IA Velocity Inlet	1300	(ml/min)
2	IA Velocity Outlet	115	(ml/min)
3	RPA Pressure Outlet	15	(mmHg)
4	LPA Pressure Outlet	15	(mmHg)
5	Offshoot Pressure Outlet	15	(mmHg)

Table 3.9 Standardized Boundary Conditions for 4.0 mm Shunts CS and KC

#	Boundary	Value	Units
1	IA Velocity Inlet	1400	(ml/min)
2	IA Velocity Outlet	140	(ml/min)
3	RPA Pressure Outlet	15	(mmHg)
4	LPA Pressure Outlet	15	(mmHg)
5	Offshoot Pressure Outlet	15	(mmHg)

Table 3.10 Standardized Average/Minimum/Max Wall Shear Values (Pa) for Each Case Study.

WSS (Pa)	AVG			MIN			MAX		
SHUNT	B1	B2	Shunt	B1	B2	Shunt	B1	B2	Shunt
KS	116.525	27.709	51.43	0.955	0.0754	3.17	400.557	221.833	249.748
JJ	105.573	14.836	45.114	1.483	0.126	0.782	303.08	59.44	175.507
KC	86.214	23.193	30.444	0.739	0.192	0.186	215.63	93.357	94.937
CS	85.88	36.649	27.766	1.48	0.222	0.294	203.056	130.258	111.294
DH	58.855	11.144	39.227	0.347	0.0451	0.0374	151.982	54.562	188.186

The results of the standardized case studies show that larger shunts (KC and CS) will have lower average and maximum WSS. It also shows that within the 3.5mm cases, the newly designed DH shunt has the superior shape for blood flow with lower average and maximum WSS. Specifically, the DH introduces entrance and exit fillets into the shunt design which are proven to improve fluid flow with the lowest WSS values of all case studies in boundaries 1 and 2.

The data for minimum values of WSS are all relatively equal in terms when compared to the magnitude of the average WSS. These minimum WSS values are also under scrutiny of various surgeons helping with this thesis due to how small they are. Typically, wall shear values under 10 Pa are known to cause stenosis within the shunt. However, the CFD program selects the node with the smallest value for the minimum for the entire named selection. Therefore, there may only be one node with such a low value. All that is known from the minimum WSS data is that there could be areas of too low wall shear or flow separation in each of the named selections.

3.3 Hess-Hoganson-Agarwal Shunt Optimization

Starting from the basis of Dr. Hoganson's DH shunt and using the case study data as a basis, the goal of this section is to create an optimized shunt that has enhanced fluid flow properties. This includes eliminating flow separation, smoothing out the transitions between high and low wall shear stress, lowering maximum wall shear stress, and equalizing the volumetric flow rate to the left and right lung.

Early on in the optimization process very drastic changes were made to the model in order to easily track the effects of changing that parameter on the overall fluid flow. Solutions from previous models

were always analyzed before the creation of any subsequent models. All model changes were tracked and monitored within excel.

After the creation of a new HHA model it is brought into ICEM and meshed utilizing both sizing and inflation functions. Named surfaces are also set so that the boundary conditions can be laid properly in the solver. On average, 5,244,463 cells are created for each model simulation.

Similar to the case studies, blood was simulated in Fluent as a Newtonian fluid with a density of 1050 kg/m^3 and viscosity of 0.00255 kg/m s. The walls of each shunt were considered smooth and rigid while the flow was assumed to be fully developed. Every HHA model was given identical boundary conditions to the 3.5mm standardized shunts: 1300 ml/min IA inflow, 115 ml/min IA outflow, and 15 mmHg PA pressure outlets.

Figures 3.31 and 3.32 show the WSS contour and centerline velocity profile for the initial HHA v1.0.0 model that was based off the initial DH design. The model retains all basic shapes of the DH shunt, however the model no longer combines two separate geometries into the shunt shape which eliminates the abrupt direction change in the middle of the shunt and seamlessly allows the shunt to transition from a smaller diameter to a larger one. However, this model is made with only a single centerline spline. Flow separation is still noticeable in the velocity contour.

Near the end of this study particle tracking within ANSYS fluent was also used to determine problem areas within geometries. Particle tracking follows an individual blood particle along its respected velocity vector. Particle tracking is useful in determining the length of time a particle will be trapped within a dead zone, if any swirling or flow separation is occurring, and how fast a particle transitions between high and low velocities.

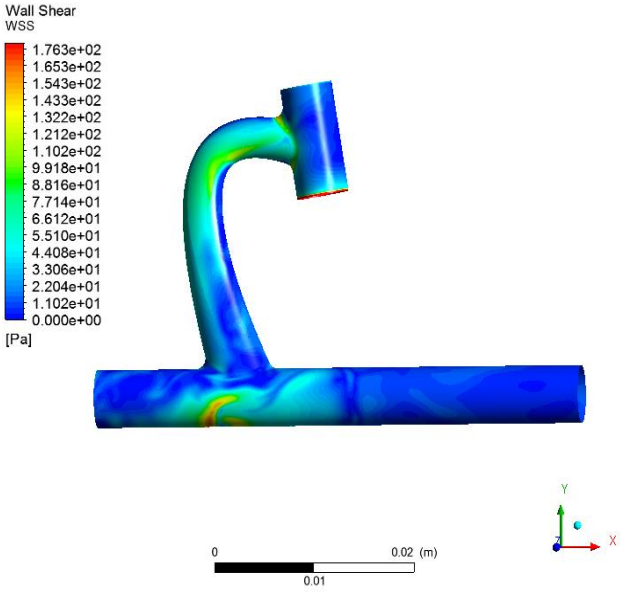

Figure 3.31 Front View WSS Contour of HHA v1.0.0

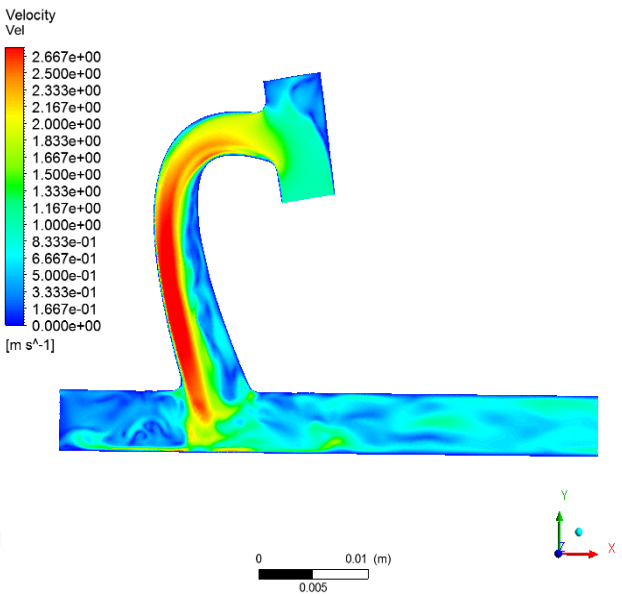

Shunt Figure 3.32 Centerline Velocity Contour of HHA v1.0.0 Shunt

In figures 3.33-3.36 the WSS contour and velocity profiles are shown from the two versions of HHA v1.1.0 shunts. In these shunts, the double spline geometry was introduced for higher customizability to the curvature and overall shape of the shunt. In HHA v1.1.0 a very exaggerated upwards bend is tested. HHA v1.1.1 lowers this exaggeration and tries to cut down on the flow separation. It is shown in these models that an upwards bend does not assist in fluid flow, but rather promotes swirling and flow separation. While v1.1.1 is able to minimize this flow separation, swirling still occurs on the top of the bend.

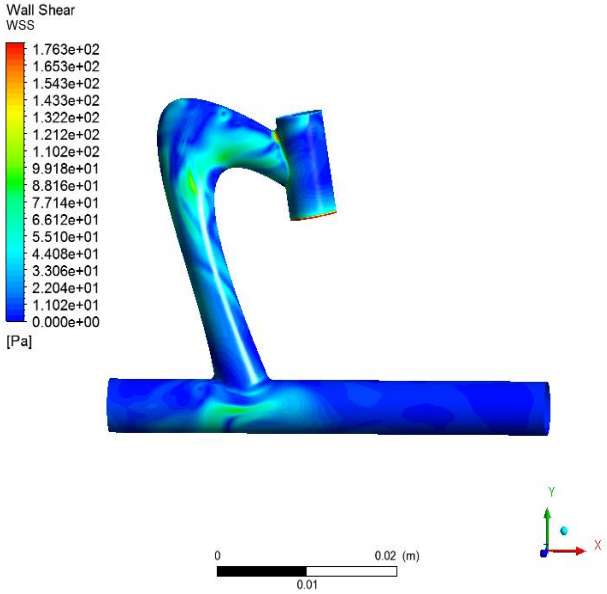

Figure 3.33 Front View WSS Contour of HHA v1.1.0 Shunt

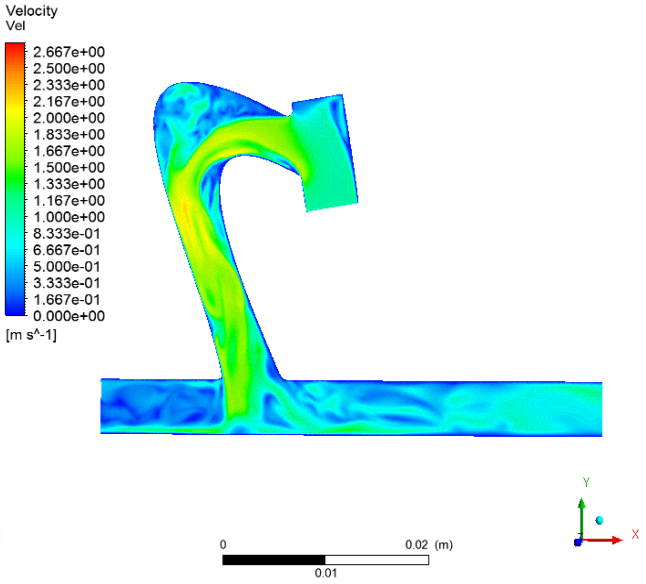

Figure 3.34 Centerline Velocity Contour of HHA v1.1.0 Shunt

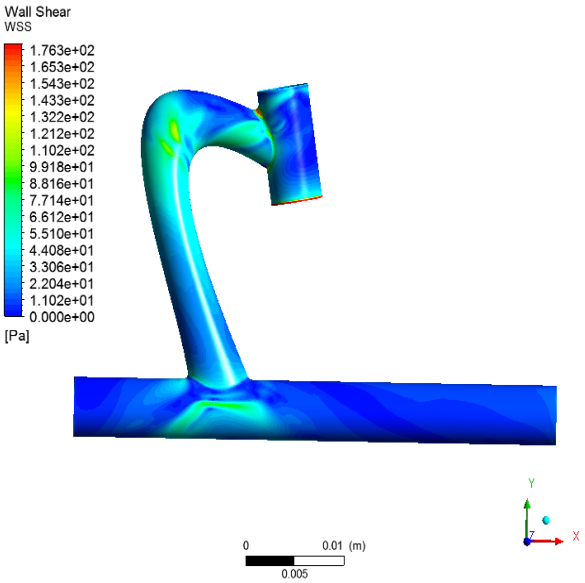

Figure 3.35 Front View WSS Contour of HHA v1.1.1 Shunt

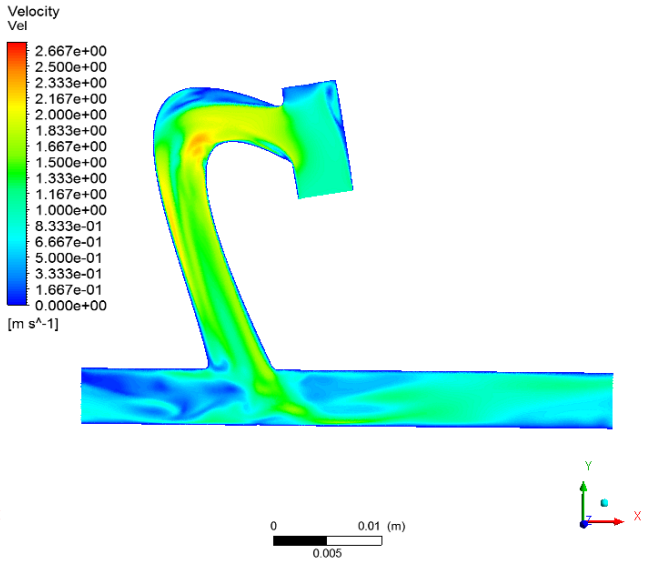

Figure 3.36 Centerline Velocity Contour of HHA v1.1.1 Shunt

Figures 3.37-3.44 show the WSS contours and velocity profiles for the four HHA v1.2.0 models. In v1.2.0 the takeoff angle is changed from 60 degrees to 80 degrees for a more horizontal shunt entrance. Subsequent models refine the curvature of shunt to reduce flow separation while increasing fillet sizes on both IA and PA boundaries. It was also noticed that the diameter of all 1.2.0 shunt models tended to be above the 4mm size throughout the length of the shunt, so v1.2.3 modified the design back into a 3.5mm shunt. This returns the design to the effective resistance range of modern shunts. HHA v.1.2.3 provided an excellent curvature for flow and low WSS but failed to tackle the problem of distributing the flow evenly to the left and right lung. It can be seen in the velocity profiles that the momentum of the fluid through the curve carries a majority of the fluid towards the left lung pulmonary exit.

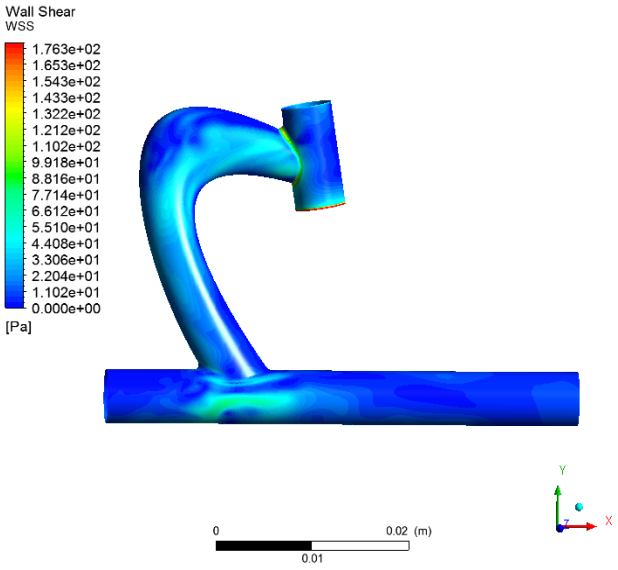

Figure 3.37 Front View WSS Contour of HHA v1.2.0 Shunt

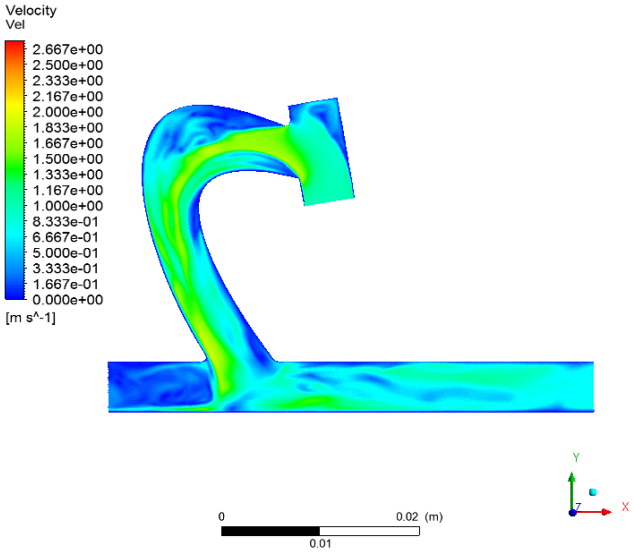

Figure 3.38 Centerline Velocity Contour of HHA v1.2.0 Shunt

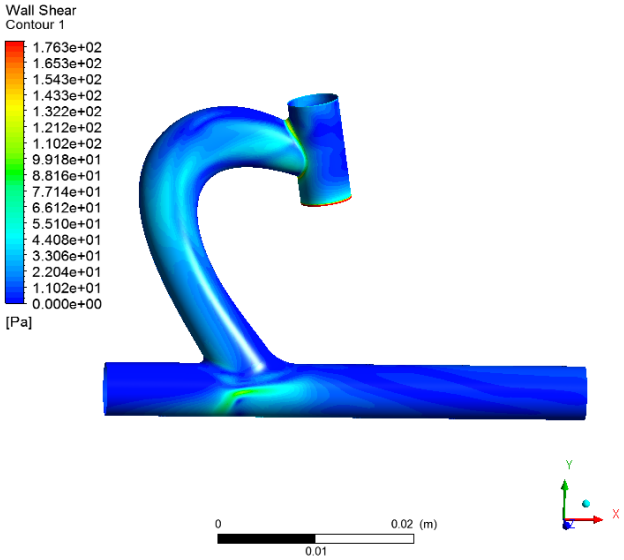

Figure 3.39 Front View WSS Contour of HHA v1.2.1 Shunt

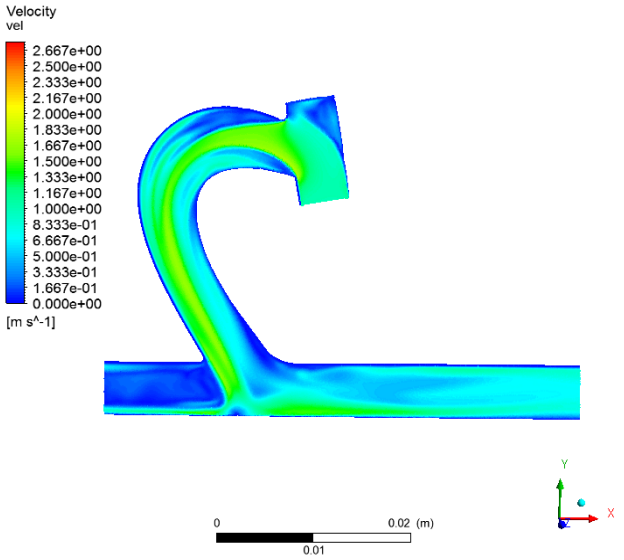

Figure 3.40 Centerline Velocity Contour of HHA v1.2.1 Shunt

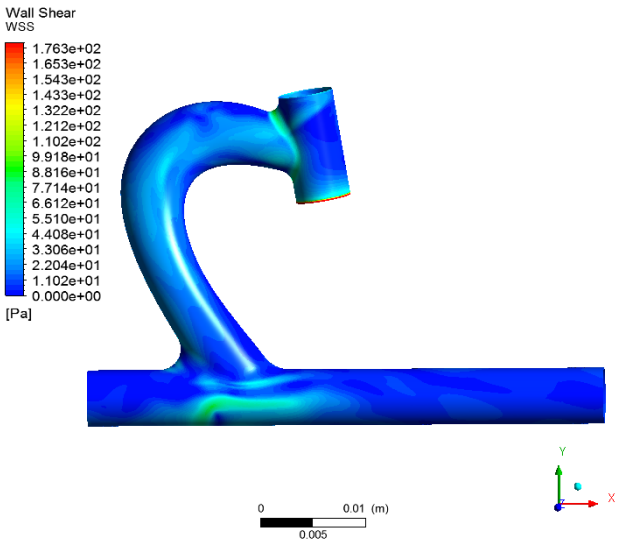

Figure 3.41 Front View WSS Contour of HHA v1.2.2 Shunt

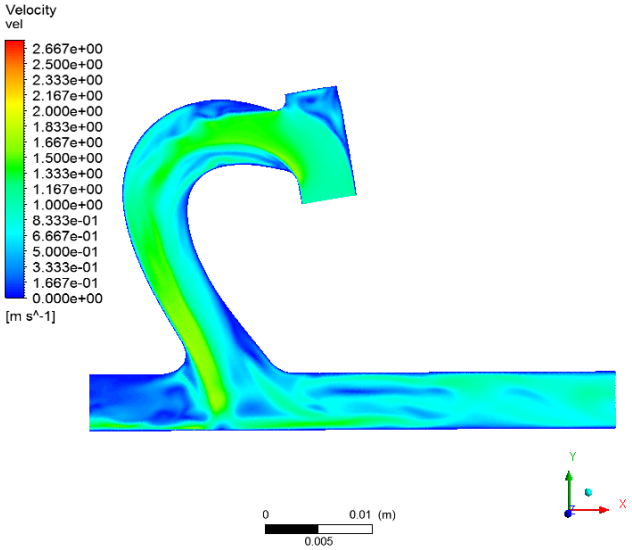

Figure 3.42 Centerline Velocity Contour of HHA v1.2.2 Shunt

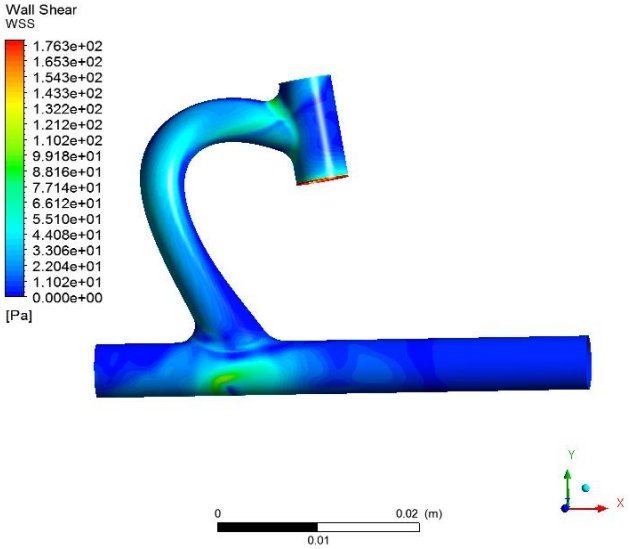

Figure 3.43 Front View WSS Contour of HHA v1.2.3 Shunt

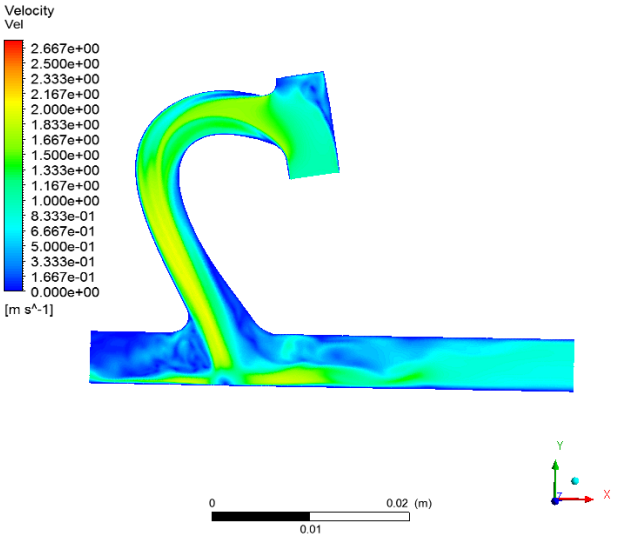

Figure 3.44 Centerline Velocity Contour of HHA v1.2.3 Shunt

The HHA v.1.3.0 models seen in Figures 3.45-3.52 attempt to split the blood flow to the left and right lung by straightening out towards the pulmonary boundary while retaining the curvature created in previous models at the top. Again HHA v1.3.2 modifies the parent design back into a 3.5mm shunt design and into the correct effective resistance range. A hypothesis of eliminating the upper fillet on the IA boundary was tested in v1.3.2. This was ultimately ineffective, proving that larger fillets on both sides of each boundary minimize the maximum WSS and eliminate sudden WSS spikes. This was reaffirmed in v.1.3.3 by increasing the IA fillets to near maximum values. While it is not shown, it is learned here that there is a maximum fillet size before sharp peaking occurs on the face of the fillet providing horrible flow cavities.

HHA v1.3.3 and v1.3.4 attempt to optimize the bottom straight curve to remove any flow separation. This design of shunt was not distributing the flow as evenly as expected so the PA fillets were adjusted up to 4x as great on the right lung side in order to encourage more flow towards that exit. This proved unsuccessful and only created a new dead zone in the PA connection.

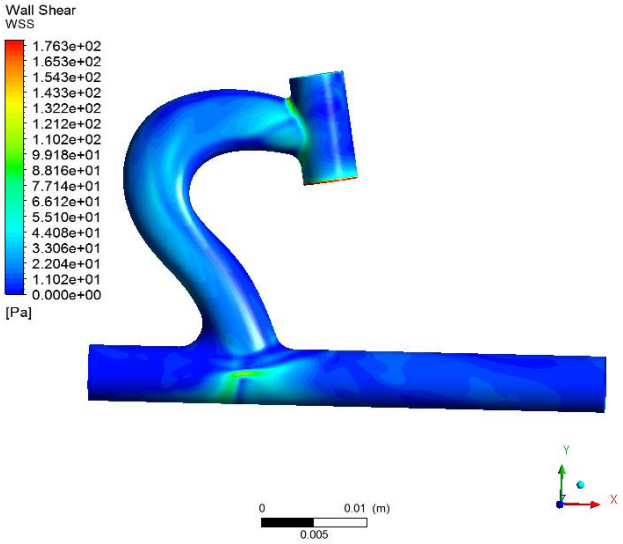

Figure 3.45 Front View WSS Contour of HHA v1.3.1 Shunt

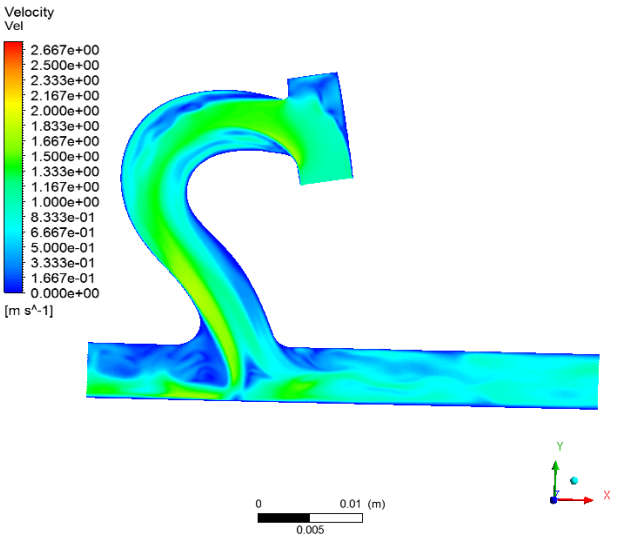

Figure 3.46 Centerline Velocity Contour of HHA v1.3.1 Shunt

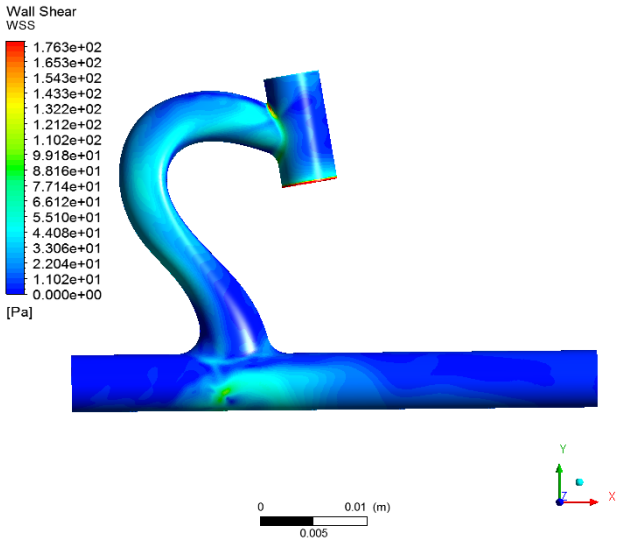

Figure 3.47 Front View WSS Contour of HHA v1.3.2 Shunt

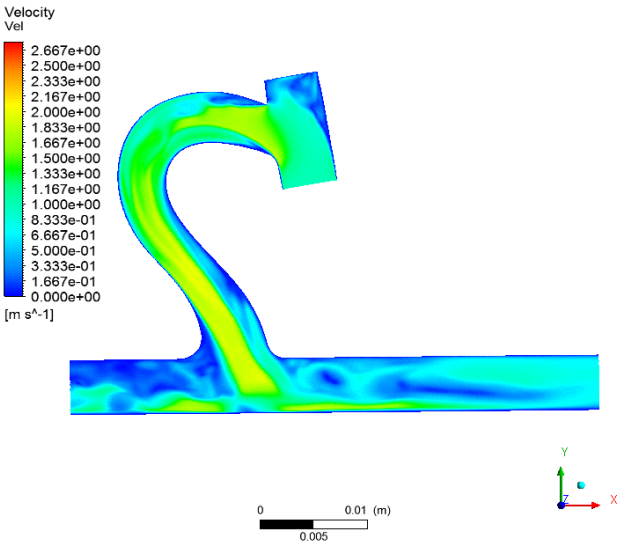

Figure 3.48 Centerline Velocity Contour of HHA v1.3.2 Shunt

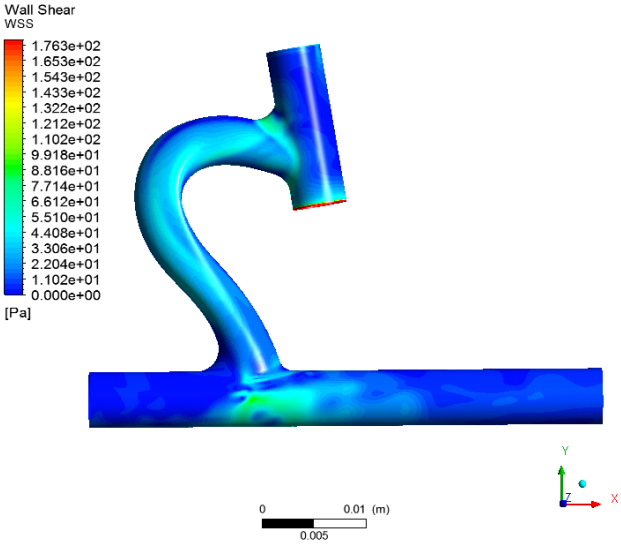

Figure 3.49 Front View WSS Contour of HHA v1.3.3 Shunt

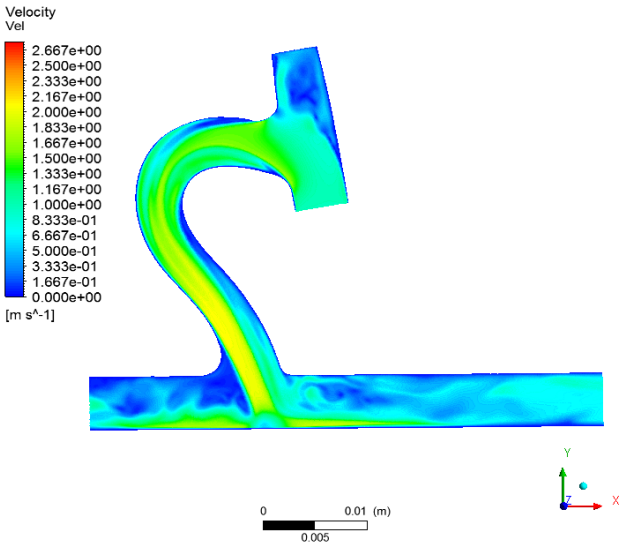

Figure 3.50 Centerline Velocity Contour of HHA v1.3.3 Shunt

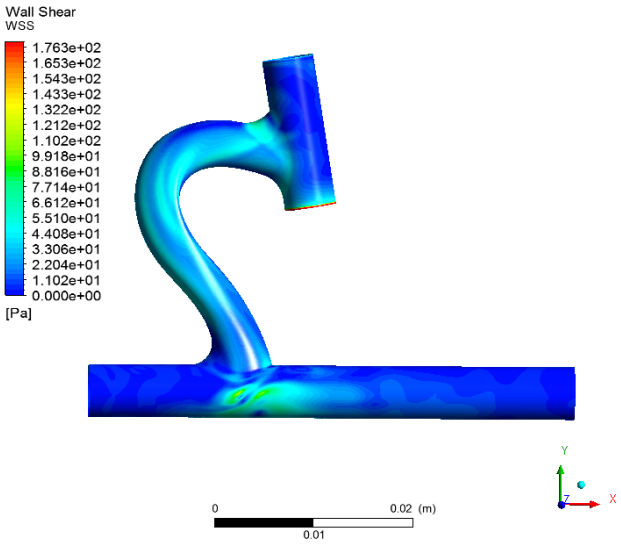

Figure 3.51 Front View WSS Contour of HHA v1.3.4 Shunt

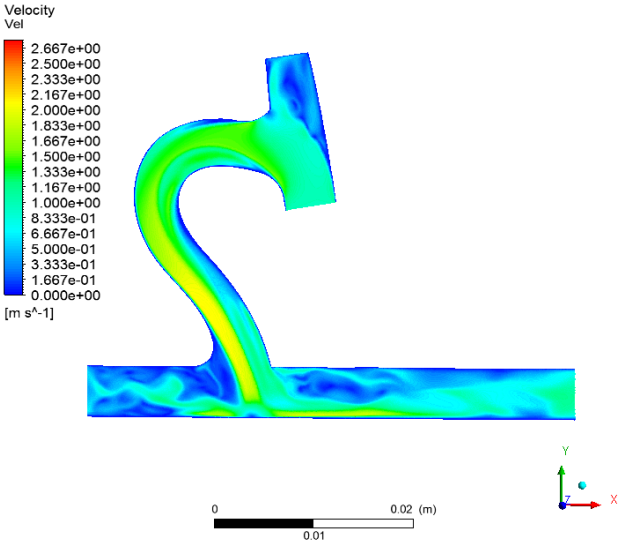

Figure 3.52 Centerline Velocity Contour of HHA v1.3.4 Shunt

In Figures 3.53-3.56 the two HHA v1.4.0 models WSS contour and velocity plots are shown. Since the '2' shape of previous models was proven unsuccessful at distributing the flow evenly a more direct straightening approach was taken. While the distribution between the left and right lung was improved, these models lacked great WSS optimization and suffer from various areas of flow separation. HHA v1.4.1 attempted to combine the old '2' shape with a straighter end but failed to provide good flow distribution. However, v.1.4.1 did prove the benefit of a large upper filler with a smaller lower fillet on the IA boundary.

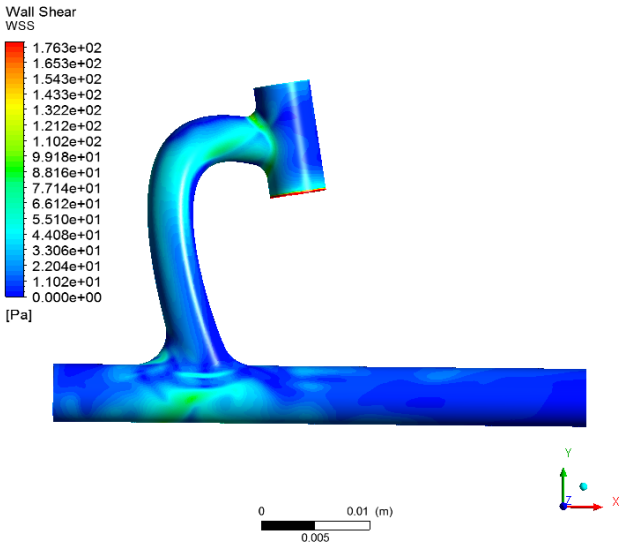

Figure 3.53 Front View WSS Contour of HHA v1.4.0 Shunt

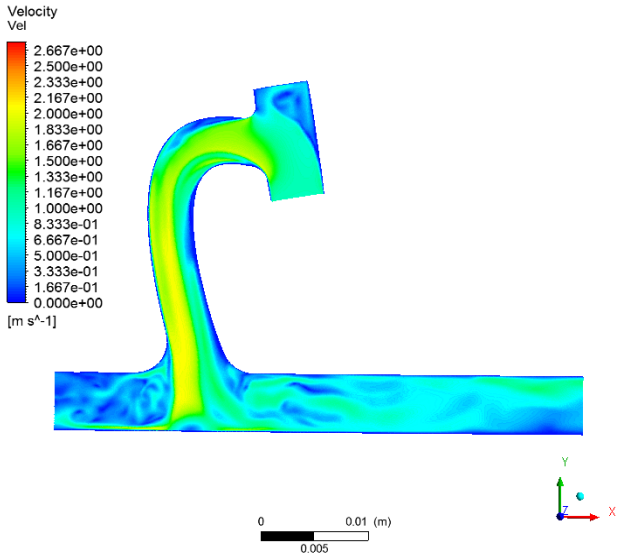

Figure 3.54 Centerline Velocity Contour of HHA v1.4.0 Shunt

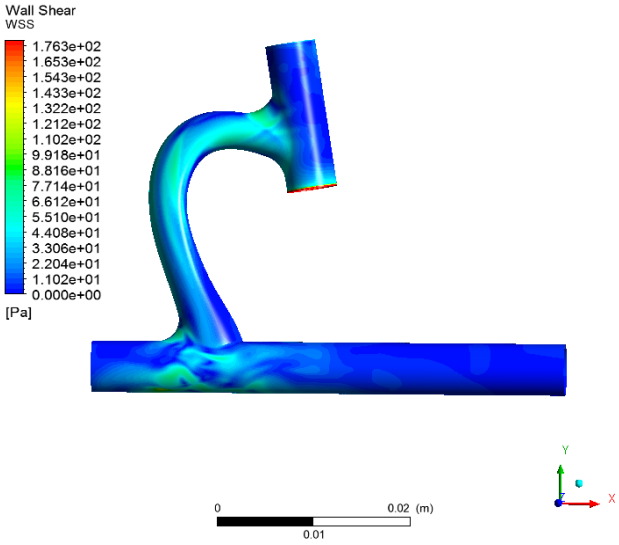

Figure 3.55 Front View WSS Contour of HHA v1.4.1 Shunt

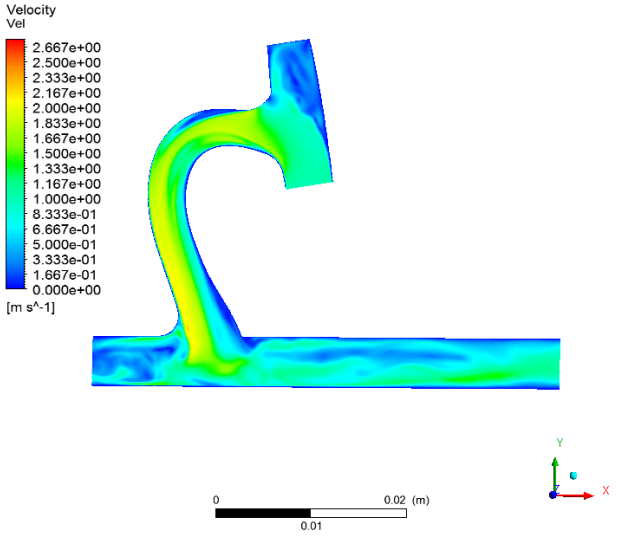

Figure 3.56 Centerline Velocity Contour of HHA v1.4.1 Shunt

Figures 3.57-3.62 show the final models of the HHA design. A lot of dicussion by various groups of doctors and engineers went into the idea for the design after analyzing all previous cases. It was decided to attemp to shorten the bend distance of the shunt by moving the PA sew in point drastically forward. This would allow for the shunt to be nearly straight after bending. This combined with the previous fillet findings were trialed in v1.5.0 and proved to have great flow distribution. However, this model contained larger amounts of WSS and flow separation. Models v1.5.1 and v1.5.2 introduced minor changes to the curve shape, exit shape, and IA fillets based on the previous model's data. HHA v1.5.2 is the current optimized model boasting minimal flow separation and the most equal flow distribution found to date.

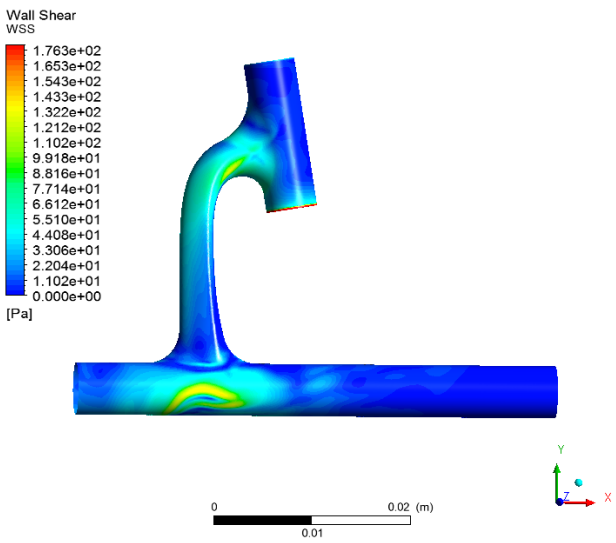

Figure 3.57 Front View WSS Contour of HHA v1.5.0 Shunt

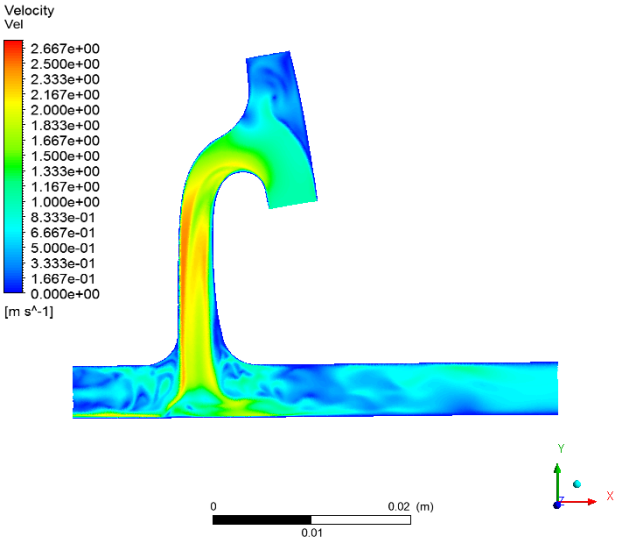

Figure 3.58 Centerline Velocity Contour of HHA v1.5.0 Shunt

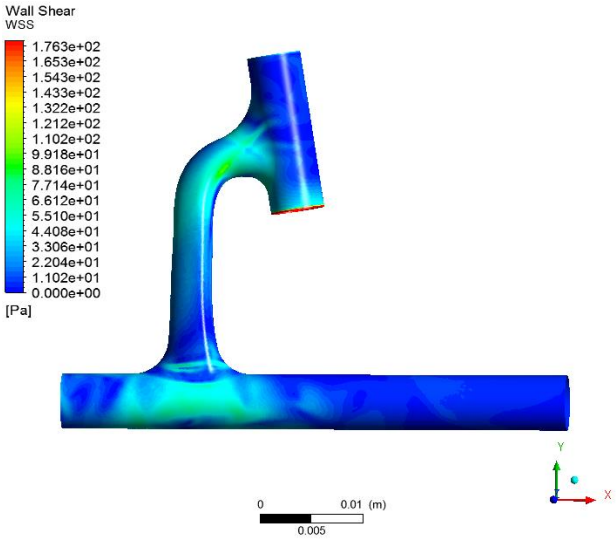

Figure 3.59 Front View WSS Contour of HHA v1.5.1 Shunt

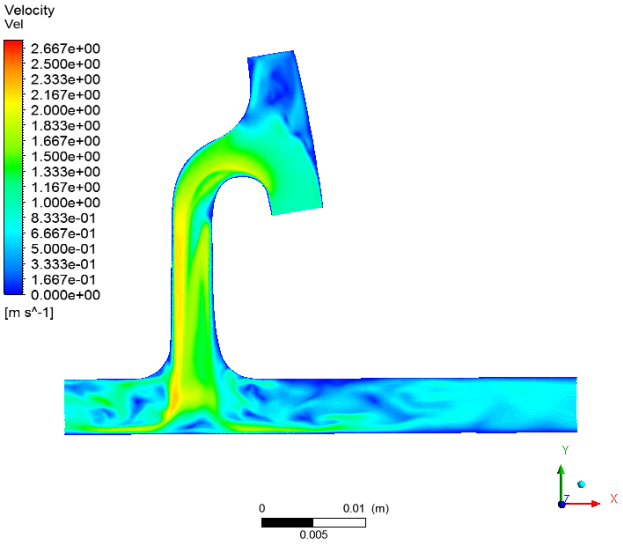

Figure 3.60 Centerline Velocity Contour of HHA v1.5.1 Shunt

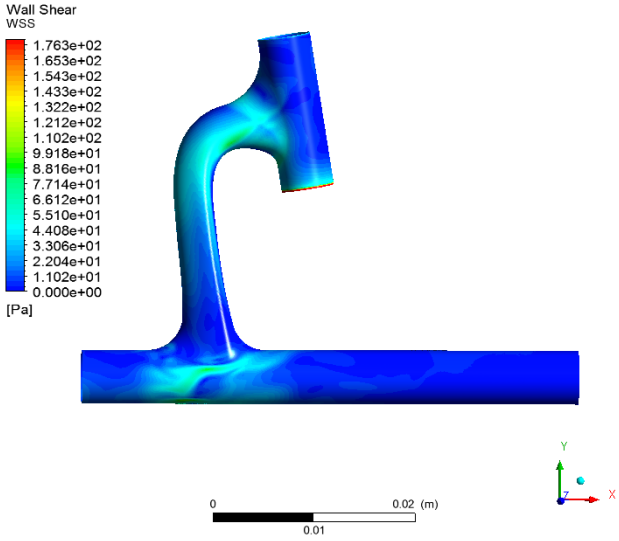

Figure 3.61 Front View WSS Contour of HHA v1.5.2 Shunt

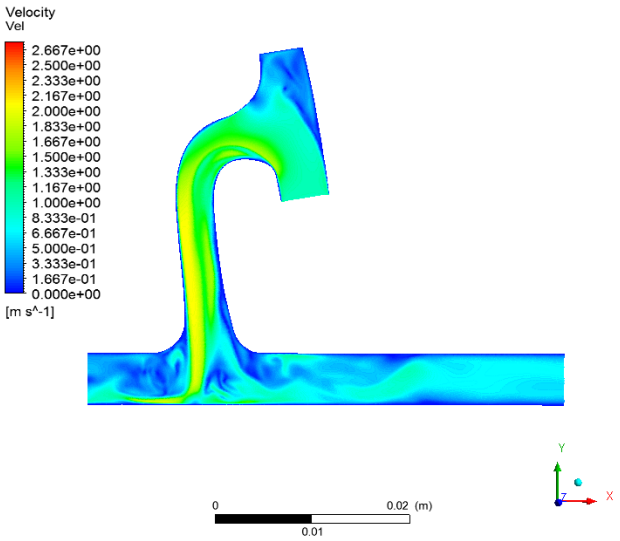

Figure 3.62 Centerline Velocity Contour of HHA v1.5.2 Shunt

3.4 Results and Validations

Tables 3.11-3.13 show the accumulated data for WSS, flow distribution, and effective resistance for each iteration of HHA model. The combination of these three charts were used during discussions over model changes and used to validate if alterations benefited or inhibited blood flow. Table 3.11 shows the great progress of lowering overall WSS as well as eliminating several areas of peak WSS. Table 3.12 expands this picture by showing why geometries with lower WSS values could not be chosen due to their inefficiency at left and right lung flow distribution. Table 3.13 validates the size, length, and flow velocity through the shunt by examining the estimated effective resistance of the overall shunt. As previously stated, current BT shunts lie within a range of 700-1100 Pa of effective resistance.

Table 3.11 Standardized Average/Minimum/Max Wall Shear Values (Pa) for Each HHA Model.

	WSS - Boundary 1 (Pa)			WSS - Boundary 2 (Pa)			WSS - Shunt Wall (Pa)			WSS - Pulmanary (Pa)		
Shunt Model Name	Facet AVG	Facet MIN	Facet MAX	Facet AVG	Facet MIN	Facet MAX	Facet AVG	Facet MIN	Facet MAX	Facet AVG	Facet MIN	Facet MAX
DH-Hess-V1.0.0	76.4565	1.0805	199.3357	27.2932	0.02583	98.6038	37.8556	0.1274	132.3314	-	-	-
DH-Hess-V1.1.0	83.154	1.55	206.4693	12.36	0.352	36.1443	25.31	0.0146	109.515	11.2	0.0378	93.876
DH-Hess-V1.1.1	93.214	1.11	231.777	25.207	0.8354	80.447	27.644	0.03797	117.121	12.138	0.04212	105.659
DH-Hess-V1.2.0	84.8884	0.77907	222.43945	16.8441	0.53077	51.68536	17.9129	0.02658	90.2289	11.8374	0.002107	89.737
DH-Hess-V1.2.1	80.364	1.1973	192.959	6.348	0.0745	38.924	17.862	0.012	75.204	11.119	0.03605	104.205
DH-Hess-V1.2.2	45.2165	0.041	121.342	11.81	0.1273	44.0509	16.67	0.01939	42.05295	11.551	0.006598	87.208
DH-Hess-V1.2.3	45.292	0.26135	124.08717	12.851901	0.12929	41.243526	23.0944	0.03025	63.16683	12.1914	0.0054144	130.211
DH-Hess-V1.3.1	55.607	0.176	185.41365	5.5716	0.0347	37.119	16.314	0.02407	58.23355	9.987	0.014337	121.4525
DH-Hess-V1.3.2	75.36	0.107468	310.58432	9.008	0.0062111	39.6266	21.52	0.034627	117.02773	11.6483	0.02057	80.236298
DH-Hess-V1.3.3	39.822	0.0577	98.9703	8.536	0.1577	71.587425	22.768	0.030117	66.559	12.6339	0.0145956	131.816
DH-Hess-V1.3.4	33.5068	0.15768	77.99277	7.497	0.06233	67.741936	23.2025	0.031826	64.670151	11.658	0.02738	116.32996
DH-Hess-V1.4.0	58.181	0.1036	149.411	16.701	0.0446	65.425	23.974	0.0289	84.423	15.468	0.075817	105.989
DH-Hess-V1.4.1	39.4616	0.3927	93.92054	25.8169	0.05903	114.34956	25.4165	0.006344	68.444383	13.6836	0.0330377	123.61048
DH-Hess-V1.5.0	34.1282	0.32295	92.0225	14.054	0.17422	76.3046	33.0455	0.030926	143.566	17.155278	0.02054	143.71924
DH-Hess-V1.5.1	33.0211	0.7144	91.291	17.9	0.05904	86.783	28.3313	0.14132	115.043256	14.8842	0.014975	158.02356
DH-Hess-V1.5.2	26.787	0.325945	99.7659	7.810411	0.052076	60.3008	22.6	0.064494	96.5597	10.647	0.0273	111.14154

Table 3.12 Flow Difference between Left and Right Lung for Each HHA Model.

Shunt Model Name	Right PA Exit Flow Rate (m3/s)	Left PA Exit Flow Rate (m3/s)	Percent Difference
DH-Hess-V1.0.0	5.66E-06	1.41E-05	85%
DH-Hess-V1.1.0	6.95E-06	1.29E-05	60%
DH-Hess-V1.1.1	6.18E-06	1.40E-05	77%
DH-Hess-V1.2.0	5.49E-06	1.44E-05	89%
DH-Hess-V1.2.1	4.75E-06	1.51E-05	104%
DH-Hess-V1.2.2	5.40E-06	1.44E-05	91%
DH-Hess-V1.2.3	5.53E-06	1.43E-05	89%
DH-Hess-V1.3.1	5.91E-06	1.40E-05	81%
DH-Hess-V1.3.2	6.79E-06	1.30E-05	63%
DH-Hess-V1.3.3	5.88E-06	1.40E-05	82%
DH-Hess-V1.3.4	6.30E-06	1.35E-05	73%
DH-Hess-V1.4.0	7.24E-06	1.26E-05	54%
DH-Hess-V1.4.1	6.44E-06	1.34E-05	70%
DH-Hess-V1.5.0	8.34E-06	1.15E-05	32%
DH-Hess-V1.5.1	8.61E-06	1.12E-05	26%
DH-Hess-V1.5.2	9.00E-06	1.09E-05	19%

Table 3.13 Estimated Effective Resistance (Pa) for Each HHA Model.

Shunt Model Name	Effective resistance (Pa)
DH-Hess-V1.0.0	1079.566741
DH-Hess-V1.1.0	689.5370655
DH-Hess-V1.1.1	487.341063
DH-Hess-V1.2.0	393.2798306
DH-Hess-V1.2.1	419.2841642
DH-Hess-V1.2.2	419.2841642
DH-Hess-V1.2.3	779.4801802
DH-Hess-V1.3.1	499.2587606
DH-Hess-V1.3.2	752.7629909
DH-Hess-V1.3.3	730.0184708
DH-Hess-V1.3.4	769.3806314
DH-Hess-V1.4.0	769.3806314
DH-Hess-V1.4.1	810.8602754
DH-Hess-V1.5.0	1098.4967
DH-Hess-V1.5.1	929.6497426
DH-Hess-V1.5.2	849.70004

The accumulation of this data along with WSS and velocity contour plots lead to the creation of the final geometry HHA v1.5.2. When compared to current day 3.5 mm shunts under the same flow conditions (standardized JJ and KS) the HHA v1.5.2 excelled at creating a smooth flow transition at the IA boundary into the shunt. The maximum WSS at this initial boundary was 99.765 Pa for v1.5.2 compared to KS's 249.748 Pa and JJ's 175.507 Pa. This is over a 42% drop in maximum WSS for both current models. The average WSS at this boundary was also dropped from 110 Pa in current shunts to 26 Pa in v1.5.2. This boundary was also successful at eliminating onset flow separation of blood first entering the shunt. The optimization of the initial innominate artery boundary was the biggest success of this thesis. Similarly to the initial boundary WSS values, the WSS in the pulmonary boundary and throughout the geometry of the shunt were lowered substantially compared to current shunts. Overall, the v1.5.2 shunt had an average WSS of 22.60 Pa compared to 51.43 Pa for the KS shunt and 45.11 Pa for the JJ shunt.

The HHA v1.5.2 model was also the most successful HHA model at distributing blood flow between the left and right pulmonary exits. HHA v.1.5.2 held a 19% percent difference in exit flow rates compared to the 80-90% range of previous HHA models. This is a great improvement to current day shunts which have great problems of over saturating one side of the lungs. Figure 3.78 illustrates the drastic differences in WSS and velocity profile between a current shunt model (KS) and the HHA v1.5.2. The figure also provides a cross section depiction of each velocity profile showing the shape variety of HHA shunts compared to current shunts.

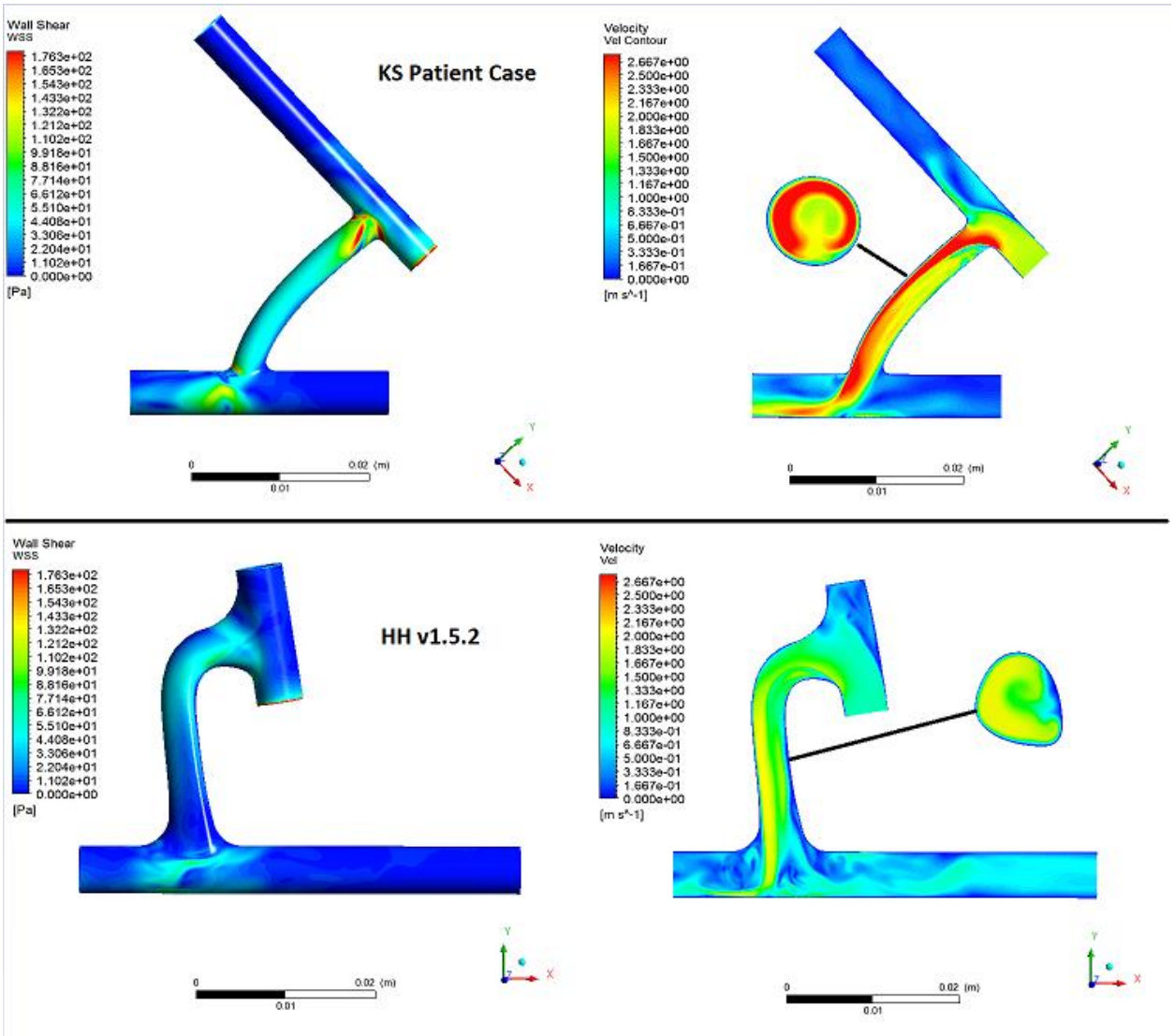

Figure 3.63 WSS Contour and Velocity Profile Comparison for the 3.5mm KS Case Study and 3.5mm HHA v1.5.2.

Chapter 4 Conclusions

An optimized BT Shunt has been created through the use of CFD to solve the governing Navier-Stokes equations with a k-kl-ω turbulence model. Five case studies were analyzed to constitute a basis of flow data for current BT shunts. WSS and flow rate values were combined with WSS contour photos and midline velocity profiles to detect areas with high risk of pulmonary vascular blockage or stenosis. These areas were adapted for increased blood flow efficiency by easing the transition between high and low WSS, lowering the maximum WSS, eliminating flow separation and distributing blood evenly between the left and right pulmonary exits. A total of 16 different iterations of designs were generated to create an optimized shape. Vastly different geometries were tested for their flow properties throughout the study.

The study of currently used shunts highlighted the areas commonly known for shunt breakdown and stenosis to occur. This study reinforced the results found by cardiovascular surgeons while promoting the importance for this research to eliminate these breakdowns. The acquired case data was used as a basis of comparison for all optimized geometries.

It was found that the IA boundary lumen that brings flow into the shunt plays a pivotal role in resultant wall shear stress values and likelihood of flow separation throughout the shunt. It was concluded that the largest fillet possible on the top side of the entrance boundary without a pointed ridge forming is best suited for optimal flow. This entrance fillet is the most important shape for controlling resulting fluid flow.

The final optimized geometry boasted over 120% drop in average WSS at the initial boundary, over 20% drop in overall average WSS, a decline of the maximum WSS by over 25%, and a 19% flow rate difference between the left and right pulmonary exits compared to current shunt models. This model also succeeded to have no symptoms of flow separation with minimal swirling and dead zones. Therefore this geometry is likely to decrease the likelihood of pulmonary blockage and stenosis occurring within the shunt and is recommended further testing for clinical practice in thoracic surgery.

Chapter 5 Future Work

Several future and ongoing projects will continue after the completion of this thesis. These include: particle tracking, fully optimizing the geometry with a genetic based algorithm, running the optimized geometry in a fluid-structure interaction simulation, adjusting the model for multiple different sizes from 3.5-4.5mm, and even study the effectiveness of the shunt within animal surgery.

Currently, individual blood particle paths through each model are being studied within fluent. Particle tracking creating a short animation of an individual particle following its respected velocity vector. This is used to analyze how long particles are getting trapped in a dead zone, how much swirling is occurring, and how fast a particle is transitioning between high and low velocity. This technology has proven very useful in determining breakdown points of shunt geometry. Vijay Govindarajan of Havard's Boston Children's Hospital has been assisting in this project.

Similar to a project done by Guangyu Bao, the optimized geometry can be ran through an actual optimization code. A genetic algorithm code could be used to create a precisely optimized shape through its ability to mimic the natural evolution process by using techniques such as inheritance, selection, crossover, and mutation [11]. Through several generations of design many untested geometries will be studied and inherited into the design naturally if they benefit the fluid flow. Genetic based optimization would be chosen over more traditional optimization algorithms due to the countless variables available for change and infinite geometric shapes.

Current work is also being done running the optimized model under a fluid-structure interaction simulation commonly called an FSI model. An FSI model is perfect for simulating vascular cases due to the ability to have moveable and deformable walls. Vessels in the body are always expanding and contracting due to fluid flow. The Gore-Tex material shunts also slightly have these elastic properties to expand and move with differing fluid flow. An FSI model would fully simulate how the shunt model would behave after surgery especially with pulsatile flows. FSI models are very popular in the study of aneurysms, myofibroblastic proliferation, and artificial vessels/organs.

This project is also planned for continuation with Dr. Hoganson who has received several grants to continue work, create a physical model, and even begin tests within animals, the first step in getting approved for clinical use. There are plans to create the optimized geometry in many different sizes specific for patient needs. Also, there are plans to create the model using tissues taken from umbilical cord after birth. This would provide the perfect synthetic material for use within the body and could mimic the properties of blood vessels better than that of Gore-Tex.

References

[1] Obstruction in Modified Blalock Shunts: A Quantitative Analysis With Clinical Correlation Winfield J. Wells, MD, R. James Yu, BS, Anjan S. Batra, MD, Hector Monforte, MD, Colleen Sintek, MD, and Vaughn A. Starnes, MD Childrens Hospital Los Angeles, Los Angeles, California

[2] Two Thousand Blalock-Taussig Shunts: A Six-Decade Experience Jason A. Williams, MD, Anshuman K. Bansal, BS, Bradford J. Kim, BA, Lois U. Nwakanma, MD, Nishant D. Patel, BA, Akhil K. Seth, BS, Diane E. Alejo, BA, Vincent L. Gott, MD, Luca A. Vricella, MD, William A. Baumgartner, MD, and Duke E. Cameron, MD

[3] "That First Operation." Medical Archives - Personal Paper Collections: Dorothea Orem Collection, www.medicalarchives.jhmi.edu/firstor.htm.

[4] "Blalock-TassigShunt." Wp.com, i2.wp.com/thoracickey.com/wp-content/uploads/2017/09/A322400_1_En_19_Fig14_HTML.gif?fit=370%2C420&ssl=1.

[5] Risk Factors for Mortality and Morbidity after the Neonatal Blalock-Taussig Shunt Procedure Petrucci, Orlando et al. The Annals of Thoracic Surgery, Volume 92, Issue 2, 642 – 652

[6] "GORE-TEX® Vascular Grafts Configured for Pediatric Shunts." Gore Medical, www.goremedical.com/products/vgpedshunt.

[7] Panday S R, Karbhase J N, Rachmale G G, Hemantkumar C J, Hishikar A A. Modified Blalock Taussig (B.T.) shunt with the use of Goretex graft. J Postgrad Med 1982;28:167-70

[8] ANSYS Inc., ANSYS 12.0 User Manual, 2012.

[9] Batchelor, G. (2000). Introduction to Fluid Mechanics.

[10] D. Keith Walters and Davor Cokljat. A three-equation eddy-viscosity model for reynolds-averaged navier-stokes simulations of transitional flows. Journal of Fluids Engineering, 130, December 2008.

[11] Bao, Guangyu, "Optimization of Blalock-Taussig Shunt and Anastomotic Geometry for Vascular Access Fistula Using a Genetic Algorithm" (2015). Engineering and Applied Science Theses & Dissertations. 108. https://openscholarship.wustl.edu/eng_etds/108

[12] D. G. Holmes and S. D. Connell. Solution of the 2D Navier-Stokes Equations on Unstructured Adaptive Grids. Presented at the AIAA 9th Computational Fluid Dynamics Conference, June, 1989.

[13] S. V. Patankar. Numerical Heat Transfer and Fluid Flow. Hemisphere, Washington, DC, 1980.

[14] Erdem, Erinc & Kontis, Konstantinos. (2010). Numerical and Experimental Investigation of transverse Injection Flows. Shock Waves. 20. 103-118. 10.1007/s00193-010-0247-1. https://www.researchgate.net/figure/Green-Gauss-node-based-gradient-evaluation-stencil_fig5_225514805

[15] Presto! Pressure Interpolation Scheme. http://ars.els-cdn.com/content/image/1-s2.0-S0021999110002275-gr1.jpg

[16] Ansys, Inc. The International Directory of Company Histories. 115. St James Press. pp. 23-25. ISBN 1558627782

[17] Munson, Bruce Roy, 1940-. Fundamentals of Fluid Mechanics. Hoboken, NJ :John Wiley & Sons, Inc., 2013. Print.

[18] Hess, Thomas and Agarwal, Ramesh K., "Computational Fluid Dynamics Analysis of Blalock-Taussig Shunt" (2017). Mechanical Engineering and Materials Science Independent Study. 56. https://openscholarship.wustl.edu/mems500/56

[19] Batchelor, G. (2000). Introduction to Fluid Mechanics.

Vita

Thomas Hess

Degrees M.S. Mechanical Engineering, Washington University in St. Louis, December 2018
B.S. Mechanical Engineering, Washington University in St. Louis, May 2018
B.S. Physics, Loyola University Chicago, May 2018

Professional Societies American Society of Mechanical Engineers
NASA Space Grant Consortium

Publications Hess, Thomas and Agarwal, Ramesh K., "Computational Fluid Dynamics Analysis of Blalock-Taussig Shunt" (2017). *Mechanical Engineering and Materials Science Independent Study*. 56. https://openscholarship.wustl.edu/mems500/56

December 2018